



Calculation of Temporal Plasmas of XFEL Experiments with a Relativistic Collisional Radiative Average Atom Code

A. J. Benita^{1,2*}

¹*Plasma Atomic Physics Group, Madrid Polytechnic University, 28006 Madrid, Spain.*

²*Department of Physics, Las Palmas Canary Islands University, 35017 Las Palmas de Gran Canaria, Spain.*

Author's contribution

The sole author designed, analyzed and interpreted and prepared the manuscript.

Article Information

DOI: 10.9734/PSIJ/2018/40246

Editor(s):

(1) Olalekan David Adeniyi, Department of Chemical Engineering, Federal University of Technology, Nigeria.

(2) Thomas F. George, Chancellor / Professor, Department of Chemistry and Physics, University of Missouri-St. Louis, Boulevard St. Louis, USA.

Reviewers:

(1) Di Rocco, Héctor Oscar, Universidad Nacional del Centro, Tandil, Argentina.

(2) Jiaolong Zeng, National University of Defense Technology, PR China.

(3) Subramaniam Jahanadan, Kolej Matrikulasi Labuan, Malaysia.

Complete Peer review History: <http://www.sciencedomain.org/review-history/23922>

Original Research Article

Received 16th January 2018
Accepted 23rd March 2018
Published 31st March 2018

ABSTRACT

In this paper, we illustrate the computational capability of the collisional radiative model ATMED CR for calculating the temporal evolution of accurate atomic populations including $n\ell j$ -splitting, mean charge and atomic processes rates. The present work contains computed time-dependent plasmas with the average atom code ATMED CR of neon and aluminium created with X-ray Free Electron Lasers proposed in the 10th Non-LTE Code Comparison Workshop. The results for plasma properties can be considered as very precise, according to the electronic temperature profiles registered in experiments of laser created plasmas with duration times of picoseconds and femtoseconds. As a consequence, the Crank-Nicholson implicit numerical iterative temporal module of ATMED CR can be considered a new rapid method for simulating this type of plasmas, avoiding some of the typical difficulties that appear in interpreting results of free electron laser experiments, as very different temporal scales in NLTE regime, enormous matrices of detailed collisional radiative codes, etc.

*Corresponding author: E-mail: anajosefa.benita@upm.es, anajosefa.benita.cerdan@alumnos.upm.es;

Keywords: Screened hydrogenic atomic model; collisional radiative average atom code; time-dependent plasmas.

1. INTRODUCTION

In a previous work [1], the collisional radiative model ATMED CR developed in the Average Atom formalism was presented. This code has been conceived to compute the population distribution of relativistic atomic levels (nj -splitting), the average ionization as well as the main atomic and radiative properties of steady-state and temporal plasmas of pure chemical elements or mixtures. The code ATMED CR described in detail inside the thesis book [2], has been developed to calculate plasma population kinetics under coronal, local or non-local thermodynamic equilibrium regimes as an extension of the module named ATMED LTE [3-5] for local thermodynamic conditions, which used the minimization of free energy to solve for the orbital populations according to the Fermi-Dirac statistics equivalent to SAHA model.

ATMED CR can perform calculations for a wide range of laboratory and theoretical conditions: optically thin or thick plasmas, photoionized plasmas with several coexistent or incident Planckian radiation fields with full or diluted intensity, plasmas created in X-ray free electron laser facilities, etc. The radiative and collisional rates for atomic processes between energy levels of the average atom are a good equilibrated set of analytical approximations of quantum mechanical ones, with a very appropriate order of magnitude by contrast with the rates between ionic charge states of detailed

models, resulting in very accurate statistical averages.

The atomic model is based on a Relativistic Screened Hydrogenic Model (RSHM) with a set of universal screening constants including nj -splitting that has been obtained by fitting to a large database of 61,350 atomic high quality data entries, compiled from the National Institute of Standards and Technology (NIST) database of U.S. Department of Commerce and from the Flexible Atomic Code (FAC). This atomic model has been specially formulated to treat ground and excited configurations of medium and highly ionized atoms [6,7].

The relativistic screening constants were calculated through ATLANTE node of the Spanish Supercomputing Network (RES). Atlante supercomputer has a cluster formed by 84 IBM JS21 blade servers with dual core PowerPC 970MP processors and 8GB RAM (336 CPUs in total), reaching 3.36 TFLOP/s and offering 96TB of storage disk. A genetic algorithm was selected as the method of optimization for adjusting simultaneously all the screening constants, using the whole set of energies included in the database of 61,350 values.

The calculation of accurate relativistic atomic populations including nj -splitting of electronic orbitals, improves the precision of atomic properties as mean charge, rates and the resolution of spectral properties as opacities and

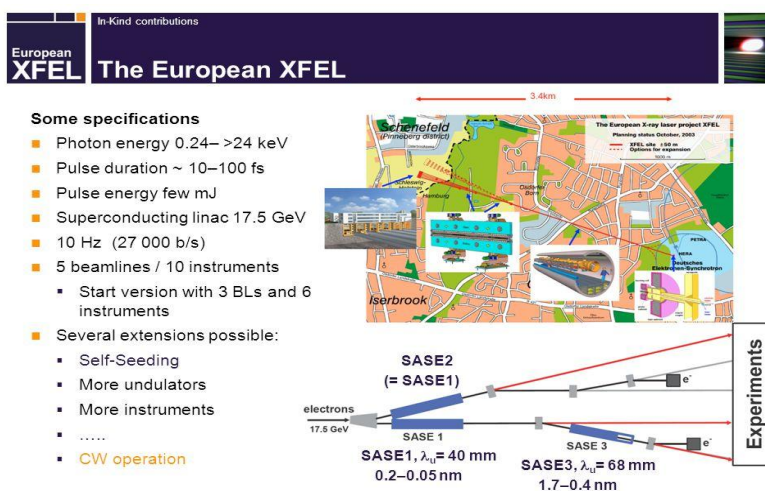


Fig. 1. The 3.4 km long European XFEL generates extremely intense X-ray flashes which are produced in underground tunnels and will allow scientists to map atomic details of viruses, film chemical reactions, and study the processes in the interior of planets

radiative power losses, with respect to collisional radiative average atom codes as XSN of W. Lokke and W. Grasberger of 1977 with n -splitting [8] or with nl -splitting [9-10].

The nlj -splitting of orbitals improves the computation of electron binding energies and radial dipole matrix elements, for calculating accurate multiplications of degeneracy and oscillator strengths gf -values and transition probabilities which represent a critical ingredient of atomic processes rates formulas, relevant for experiments in X-ray free electron laser facilities as collisional excitation, deexcitation and collisional ionization, three body recombination as well as autoionization and dielectronic capture.

In Section 2 we model with ATMED CR neon and aluminium temporal plasmas created in X-Ray Free Electron Laser facilities (Fig. 1), proposed in the 10th Non-LTE Code Comparison Workshop [11] of interest for several fields of research in high energy density physics as laser-matter interaction. Section 3 explains in detail the process of developing the code ATMED CR and how the contrast with results within more than 380 references has been carried out carefully to know better what accuracy this code can achieve. Section 4 contains main conclusions.

2. MODELING OF TIME DEPENDENT PLASMAS

2.1 Temporal Resolution of Average Atom Equations inside ATMED CR Code

This method supposes that in each time interval ionization equilibrium is not necessarily reached, so that the plasma thermodynamic parameters changes of temperature, density, etc., take place more rapidly than some atomic processes characteristic times.

The temporal discretization is carried out through applying the Crank Nicholson method in which the temporal derivative of a variable a can be expressed as:

$$\frac{da}{dt} = -\omega a \Rightarrow \frac{a^{t+\Delta t} - a^t}{\Delta t} = -\omega \left(\theta a^{t+\Delta t} + (1-\theta)a^t \right) \quad (1)$$

Where a^t and $a^{t+\Delta t}$ represent the values of the variable in two instants characterized by times t and $t + \Delta t$, respectively, being Δt the time step of the kinetic calculation.

The parameter $0 \leq \theta \leq 1$ characterizes with its value the type of solution, so that $\theta = 0$ if the

solution is totally explicit and $\theta = 1$ if the solution is totally implicit.

For other intermediate value the solution will be explicit-implicit. Particularizing for kinetic equations of average atom relativistic populations and considering the totally implicit solution $\theta = 1$, it is obtained the next set of equations for temporal intervals ($m = t_0, t_1, t_2, \dots, t_m, t_{m+1}, \dots, t_{\text{end}}$) and with iterations of populations 1, 2, ..., p , $p+1$, ..., inside each temporal interval considering a total time duration of $\tau = N\Delta t : 0 \rightarrow N\Delta t$:

$$\begin{aligned} \frac{\overline{P_i^{t+\Delta t}} - \overline{P_i^t}}{\Delta t} &= -\omega \overline{P_i^{t+\Delta t}} = (D_i^{t+\Delta t} - \overline{P_i^{t+\Delta t}}) S_i^{t+\Delta t} - \overline{P_i^{t+\Delta t}} L_i^{t+\Delta t} \\ \overline{P_i^{t+\Delta t}} &= \overline{P_i^t} + \Delta t * \left[(D_i^{t+\Delta t} S_i^{t+\Delta t} - \overline{P_i^{t+\Delta t}} S_i^{t+\Delta t}) - \overline{P_i^{t+\Delta t}} L_i^{t+\Delta t} \right] \\ \overline{P_i^{t+\Delta t}} + \Delta t * \overline{P_i^{t+\Delta t}} S_i^{t+\Delta t} + \Delta t * \overline{P_i^{t+\Delta t}} L_i^{t+\Delta t} &= \overline{P_i^t} + \Delta t D_i^{t+\Delta t} S_i^{t+\Delta t} \\ \overline{P_i^{t+\Delta t}} \left(1 + \Delta t * S_i^{t+\Delta t} + \Delta t * L_i^{t+\Delta t} \right) &= \overline{P_i^t} + \Delta t D_i^{t+\Delta t} S_i^{t+\Delta t} \\ \overline{P_i^{t+\Delta t}} \Big|_{p+1} &= \frac{\overline{P_i^t} + \Delta t * D_i^{t+\Delta t} S_i^{t+\Delta t}}{\left(1 + \Delta t * S_i^{t+\Delta t} + \Delta t * L_i^{t+\Delta t} \right)} \Big|_p \quad (2) \end{aligned}$$

Being:

- $D_i \equiv g_i$: Degeneracy affected by pressure ionization of relativistic orbital i .
- L_i : Sum of coefficients corresponding to depopulation of energy level i .
- P_i : Fractional population of relativistic orbital i .
- S_i : Sum of coefficients corresponding to population of energy level i .

In the previous situation to $t = 0$ s (temporal interval $m = t_0$), that's to say, in the situation previous to the initial one, it is supposed that the plasma is in specific conditions of density and temperature in a way that starting in $t = 0$ s density and temperature variations take place more rapidly than the characteristic times of some atomic processes. In the first temporal interval the stationary collisional radiative balance is solved in order to start with correct values of plasma properties:

$$\overline{P_i^{p+1}} = \frac{D_i}{1 + \frac{L_i}{S_i}} \Big|_{\overline{P_i} = \overline{P_i^p}} \quad (3)$$

Considering a time duration of $\tau = N\Delta t : 0 \rightarrow N\Delta t$, specific conditions of temperature, density, etc., are associated to each interval:

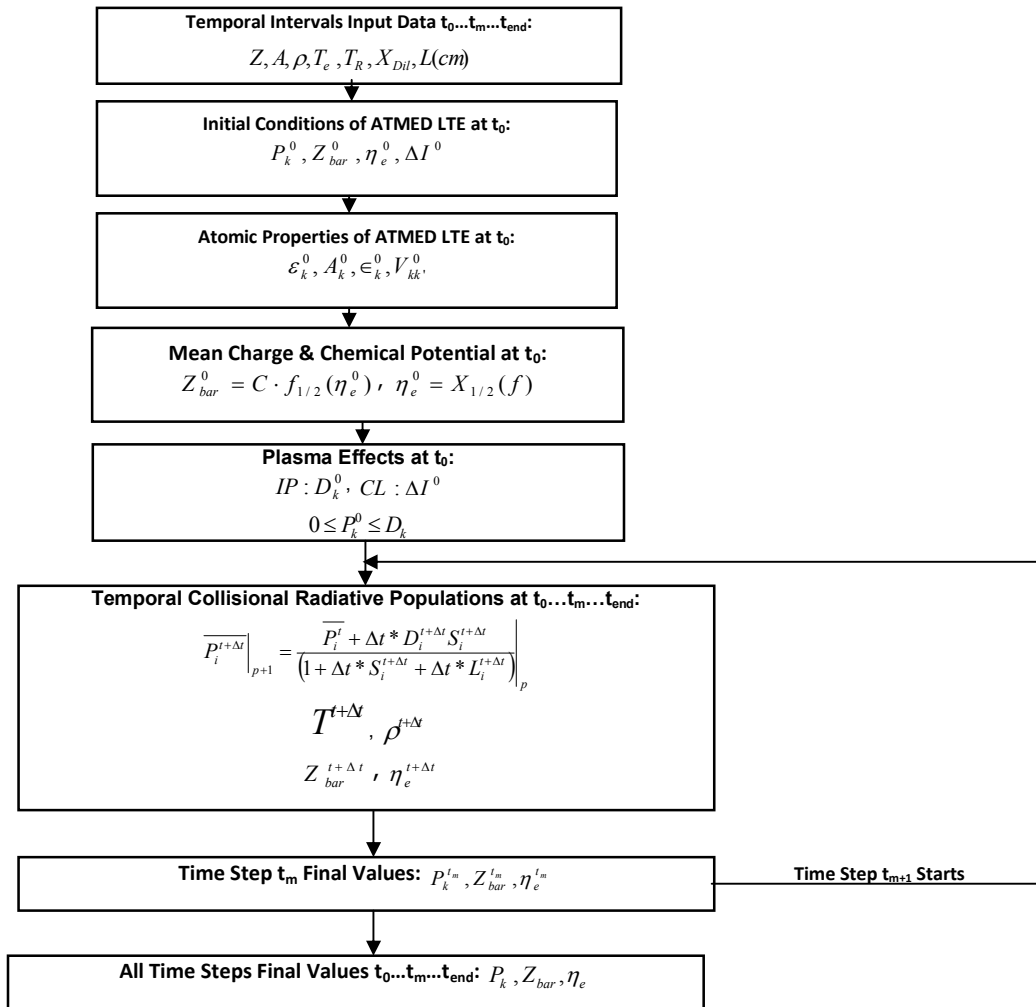
$$\begin{aligned} \Delta t : 0 \rightarrow \Delta t = \Delta t - 0 &\Rightarrow T^{\Delta t}, \rho^{\Delta t} \\ 2\Delta t : \Delta t \rightarrow 2\Delta t = 2\Delta t - \Delta t &\Rightarrow T^{2\Delta t}, \rho^{2\Delta t} \dots \\ N\Delta t : (N-1)\Delta t \rightarrow N\Delta t = N\Delta t - (N-1)\Delta t &\Rightarrow T^{N\Delta t}, \rho^{N\Delta t} \end{aligned}$$

This way the plasma parameters are recalculated when the code advances a time step with the new conditions of density, temperature, etc. The time step of the kinetic computation of populations, totally determines the evolution of plasma parameters. In the FORTRAN code it is considered the totally implicit solution $\theta = 1$ for the temporal resolution of equations. In whatever temporal interval different from the first one of the grid, the solution for populations is as follows:

$$\left. \overline{P_i^{t+\Delta t}} \right|_{p+1} = \frac{\overline{P_i^t} + \Delta t * D_i^{t+\Delta t} S_i^{t+\Delta t}}{\left(1 + \Delta t * S_i^{t+\Delta t} + \Delta t * L_i^{t+\Delta t} \right) \Big|_p} \quad (4)$$

Although it is less complex than other temporal codes as the one described in section "III. ATOMIC PHYSICS AND NUMERICAL METHOD" of the Reference [12], because of being based on the implicit numerical method of Crank Nicholson, the temporal model ATMED CR ends up being very agile in the fast resolution of the collisional radiative balance in each temporal interval, characterized by specific thermodynamic conditions, and linking conveniently the populations of each relativistic orbital in every time interval with respect to the previous one.

The detailed explanation of operating schemes of the code can be found in Reference [2]. For solving the temporal collisional radiative balance of ATMED CR it is used the next iterative loop:



The description of parameters of the average atom representing the whole plasma is as follows:

- A_k : External screening of electrons in outer orbitals with respect to the one considered k .
- $D_k \equiv g_k$: Degeneracy affected by pressure ionization of relativistic orbital k .
- $D_k^0 = 2j+1$: Maximum degeneracy or statistical weight of relativistic orbital k .
- $I_i = -\epsilon_i \text{ eV}$: Ionization potential of relativistic level i .
- $L \equiv D$: Plasma characteristic length in cm.
- L_i : Sum of coefficients corresponding to depopulation of energy level i .
- P_k : Fractional population of relativistic orbital k .
- Q_k : Screened charge of relativistic orbital k .
- S_i : Sum of coefficients corresponding to population of energy level i .
- $T_e \equiv T \text{ eV}$: Electronic temperature.
- $T_R \equiv T_{rad} \text{ eV}$: Radiation temperature.
- V_{ik}, V_{jk} : Electronic interaction energies between orbitals (i, k) and (j, k) which represent the variation of energy in level i or j when an electron is added to level k .
- X_{Dil} : Dilution factor.
- Z_{bar} : Mean charge.
- $\beta = 1/k_B T$: Inverse of temperature.
- $\epsilon_i \text{ eV}$: Energy eigenvalue of Dirac's equation of relativistic orbital i .
- $\epsilon_i \text{ eV}$: Energy of relativistic orbital i in the average atom configuration.
- $\epsilon_{ij} = \epsilon_j - \epsilon_i \text{ eV}$: Excitation energy between relativistic orbitals i and j .

- η_e : Reduced electronic chemical potential.
- $\sigma_{kk'}$: Screening constant between relativistic orbitals k and k' .
- Δ : Ionization potential or binding energy change because of continuum lowering.

2.2 Application of Temporal Resolution of Average Atom Equations in ATMED CR

2.2.1 X-ray free electron laser experiments general description

To interpret the results of XFEL's – Plasma interaction experiments, there are difficulties in how to account for these three components, atomic physics, radiation transport and plasma physics [13]. The main problems for simulating the temporal plasmas created in these facilities are the following:

- Non linear and complex plasmas and interpretation of experimental data.
- Very different temporal scales in NLTE regime.
- Enormous matrices of detailed collisional radiative codes.
- Numerical simulation at high scale.

In the next subsections there are displayed data of calculations with the code ATMED CR of neon and aluminium plasmas proposed in the Workshop NLTE-10 [11], see Table 1, considering only electronic temperature T_e and electronic density N_e temporal profiles at constant ionic density N_{ion} , because simultaneous temporal evolutions of radiation temperature T_R or dilution factor X_{dil} have not been provided. So it is supposed in calculations that the radiation energy created by the laser causes very rapid changes in electronic temperature according to the environment of the experiments in the XFEL's facilities. Nevertheless, ATMED CR could perform calculations considering simultaneous evolutions of several thermodynamic variables versus time $T_e(t)$, $N_e(t)$, $N_{ion}(t)$, $\rho(t)$, $T_R(t)$, $X_{dil}(t)$, etc.

Considering the characteristic times of experiments in comparison with times of the atomic processes rates, the calculations are very accurate because the collisional radiative balance of ATMED CR is a statistical average of the results of detailed models, even for durations

of laser irradiation of $8.0E-14$ s for aluminium or of $3.4E-13 \div 2.3E-13$ s for neon. The temporal resolution provides information about the order of magnitude of processes rates, atomic and radiative properties characterizing the specific plasma evolution of conditions for each time interval.

2.2.2 Temporal plasmas of neon

The results for neon plasma properties can be considered as very precise, according to the

electronic temperature profiles provided by experiments of laser created plasmas in the Linac Coherent Light Source [14] (LCLS of Fig. 2) with radiation energies of E_{rad} (eV) = 800, 1050, 2000 and of duration times of $3.4E-13$, $2.8E-13$ and $2.3E-13$ s respectively, see Table 1. These experiments have been carried out for exploring the interactions of high-intensity, hard X-rays with matter. Understanding how electrons in matter respond to ultra-intense X-ray radiation is essential for all applications.

Table 1. Main parameters of XFEL experiments of optically thin plasmas of neon and aluminium

Z	N_{ion} (ion/cm ³)	ρ (g/cm ³)	E_{rad}^a (eV)	Bandwidth (eV)	Intensity (W/cm ²)	Field (J/cm ² /s/Hz/rad)	Duration (s)
10	1.0E+18	0.000034	800	4	2.35E+17	19.4	3.40E-13
10	1.0E+18	0.000034	1050	4	2.86E+17	23.5	2.80E-13
10	1.0E+18	0.000034	2000	4	3.48E+17	28.6	2.30E-13
13	6.0E+22	2.688233	1580	4.4	1.17E+17	8.73	8.00E-14
13	6.0E+22	2.688233	1650	4.4	9.34E+16	6.99	8.00E-14

^a E_{rad} : Radiation Energy.

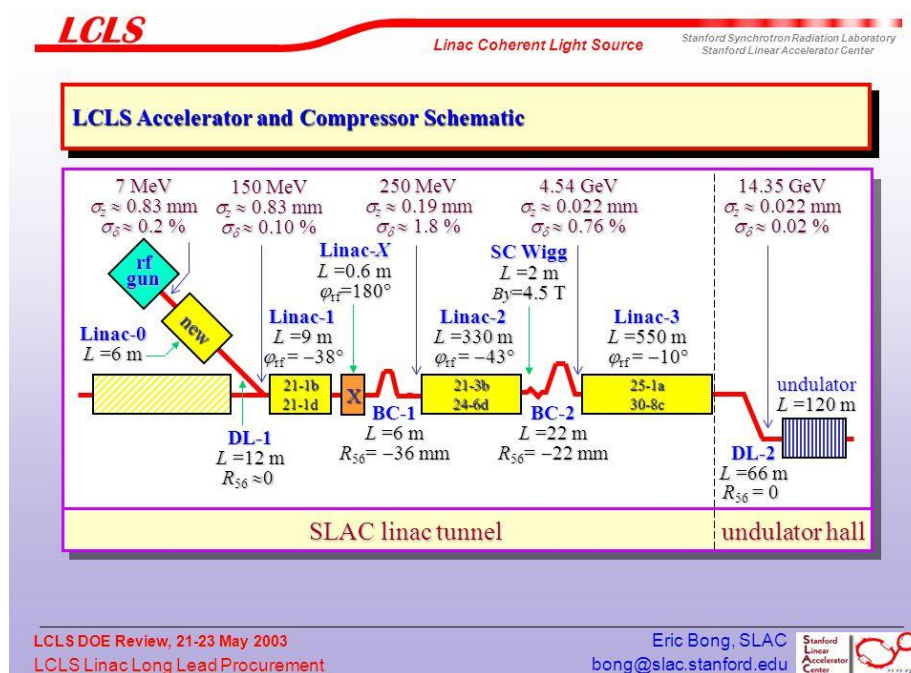


Fig. 2. The Linac Coherent Light Source at SLAC takes X-ray snapshots of atoms and molecules at work, revealing fundamental processes in materials, technology and living things. LCLS is a Science Facility operated for the U.S. Department of Energy by Stanford University

According to the temporal electronic temperature profiles provided in the NLTE-10 Workshop, the time step is variable $\Delta t(t)$ and the grid of nodes for temporal intervals ($m = t_0, t_1, \dots, t_m, t_{m+1}, \dots, t_{\text{end}}$) has been selected considering the next formula adapted from the Equation (4):

$$\overline{P_i^{t+\Delta t}} \Big|_{p+1} = \frac{\overline{P_i^t} + \Delta t^{t+\Delta t} * D_i^{t+\Delta t} S_i^{t+\Delta t}}{\left(1 + \Delta t^{t+\Delta t} * S_i^{t+\Delta t} + \Delta t^{t+\Delta t} * L_i^{t+\Delta t}\right) \Big|_p} \quad (5)$$

The calculations with ATMED CR in order to account for dense plasma effects, have been performed with the formulas belonging to Stewart-Pyatt Continuum Lowering and Ionization Pressure models, the last one being very similar to Ecker-Kröll model.

The formulas for these models of plasma effects are the next ones:

- Pressure ionization D_k :

$$D_k = \frac{2j_k + 1}{1 + \left(a_{zm} \frac{r_k^0}{R_i}\right)^{b_{zm}}} \quad (6)$$

The values D_k are considered in all rate equations, that's to say the degeneracy of the relativistic subshell k affected by pressure ionization.

- a_{zm} & b_{zm} : Tabulated parameters [3].
- r_k^0 : Radius of relativistic orbital k of isolated neutral atom.
- $R_i = \left(\frac{4\pi \rho N_A}{3 A}\right)^{-1/3}$: Ion sphere radius depending on Avogadro's number N_A , density ρ and molecular weight A .
- Continuum lowering, the values $D_k^0 = 2j_k + 1$ are considered in all rate equations, that's to say the maximum degeneracy of the relativistic subshell, following Stewart-Pyatt's formula with temperature T in atomic units (ua) and N_i as ionic density [3,5]:

$$D_e = \sqrt{\frac{T(ua)}{4\pi Z_{bar}^2 N_i}} \quad (7)$$

$$D_i = \sqrt{\frac{T(ua)}{4\pi Z_{bar}^2 N_i}} \quad (8)$$

$$R_D = \frac{D_i * D_e}{\sqrt{D_i^2 + D_e^2}} \quad (9)$$

$$\Delta I = \frac{1}{2} \frac{Z_{bar}}{R_i} \left[\left(1 + \left(\frac{R_D}{R_i} \right)^3 \right)^{\frac{2}{3}} - \left(\frac{R_D}{R_i} \right)^2 \right] \quad (10)$$

- ΔI : Ionization potential or binding energy change because of continuum lowering.

Considering continuum lowering according to Stewart-Pyatt model in the collisional radiative balance calculations, it is obtained a slightly higher value of mean charge for all instants, see Fig. 3.a. More data computed with ATMED CR are collected in APPENDIX A. The formulas of both formalisms can be considered as valid because of reproducing with high accuracy experimental values.

We can observe also in Fig. 3.b, that n-shell populations temporal evolutions $P_n(t)$ at $E_{\text{rad}}=800$ eV and $P_n(t)$ n-shells populations temporal evolutions at $E_{\text{rad}}=1050$ eV versus 2000 eV, follow perfectly the changes in the electronic temperature temporal profiles.

2.2.3 Temporal plasmas of aluminium

The results for aluminium plasma properties can be considered as very precise, according to the electronic temperature profiles provided by experiments of laser created plasmas in the Linac Coherent Light Source (LCLS) [15] with radiation energies of E_{rad} (eV) = 1580, 1650 and with duration times of $8.0E-14$ s, see Table 1. These experiments have been carried out for making direct measurements of the ionization potential depression in dense plasmas and for analyzing the predictions made with the formulas belonging to Stewart-Pyatt or Ecker-Kröll models. The calculations with ATMED CR have been made with the formulas of Ionization Pressure model.

As a direct consequence of the relativistic splitting of matter structure included in ATMED CR code and the high sensitivity to slight changes in the experiment characteristics (E_{rad} , intensity, $T_e(t)$, etc.), in Fig. 4 we can accurately observe the instant of time at around which it

takes place the saturation of energy levels depopulation, which in turn is the same instant at which the mean charge begins to remain practically constant with a graphically almost horizontal evolution. In Fig. 4, the aforementioned instant respectively occurs at $1.530E-13$ s with E_{rad} (eV) = 1580 or at $1.360E-13$ s with E_{rad} (eV) = 1650, being in consequence the gap between dashed lines representing the evolution of populations, narrower at several instants for 1650 eV than for 1580 eV.

We can check also in Fig. 4.a, that considering imaginary horizontal lines at all n-shells ($n=1\div6$), it is rapidly noticed that at the end of experiments at instant $1.670E-13$ s, the small difference in final mean charges $Z_{bar} = 7.375325 / 7.893010$ belonging respectively to E_{rad} (eV) = 1580/1650, corresponds fundamentally to the slight difference in population of n=2-shell, $2.972565E+00 / 2.554551E+00$. See in Table 2 with more detail the populations of relativistic levels $2s_{1/2}$, $2p_{1/2}$ and $2p_{3/2}$.

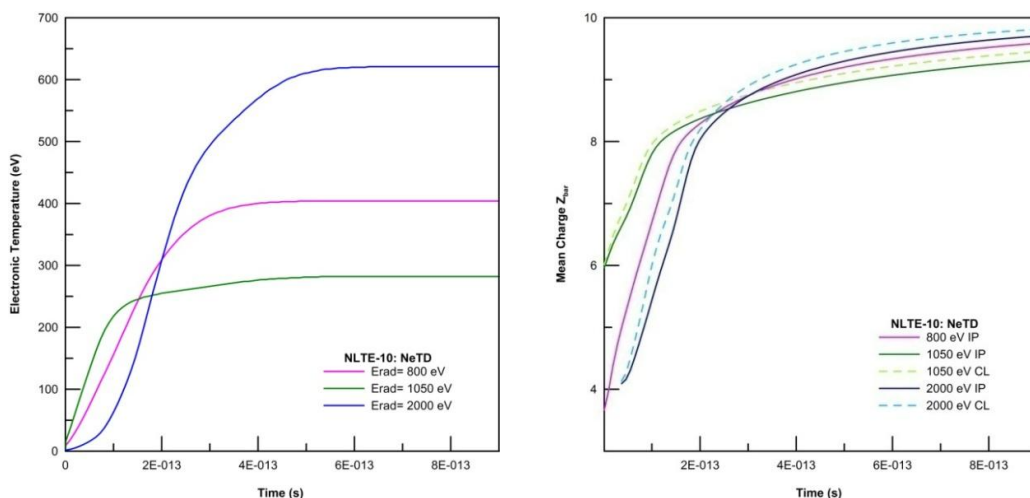


Fig. 3.a. Calculations with the code ATMED CR of neon plasmas proposed in the 10th Non-LTE Code Comparison Workshop, from left to right graphs: electronic temperature temporal profile $T_e(t)$ of the experiments at X-ray free electron laser facilities as LCLS [11]; mean charge temporal evolution $Z_{bar}(t)$ with the formulas belonging to Stewart-Pyatt Continuum Lowering CL and Ionization Pressure IP models, the last one being very similar to Ecker-Kröll model

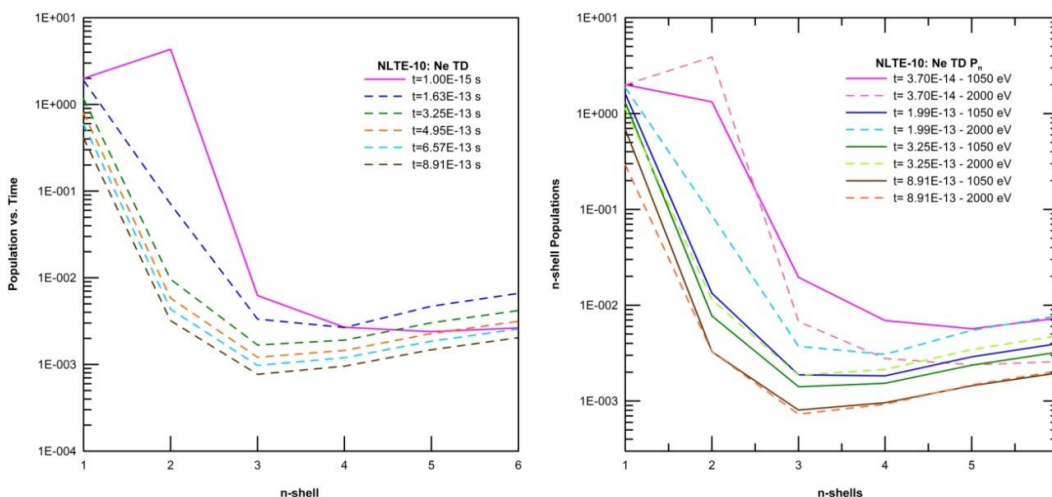


Fig. 3.b. Calculations with the code ATMED CR of neon plasmas proposed in the 10th Non-LTE Code Comparison Workshop, from left to right graphs: n-shell populations temporal evolution $P_n(t)$ at $E_{rad}=800$ eV and n-shell populations temporal evolution $P_n(t)$ at $E_{rad}=1050$ eV versus 2000 eV for representative temporal intervals

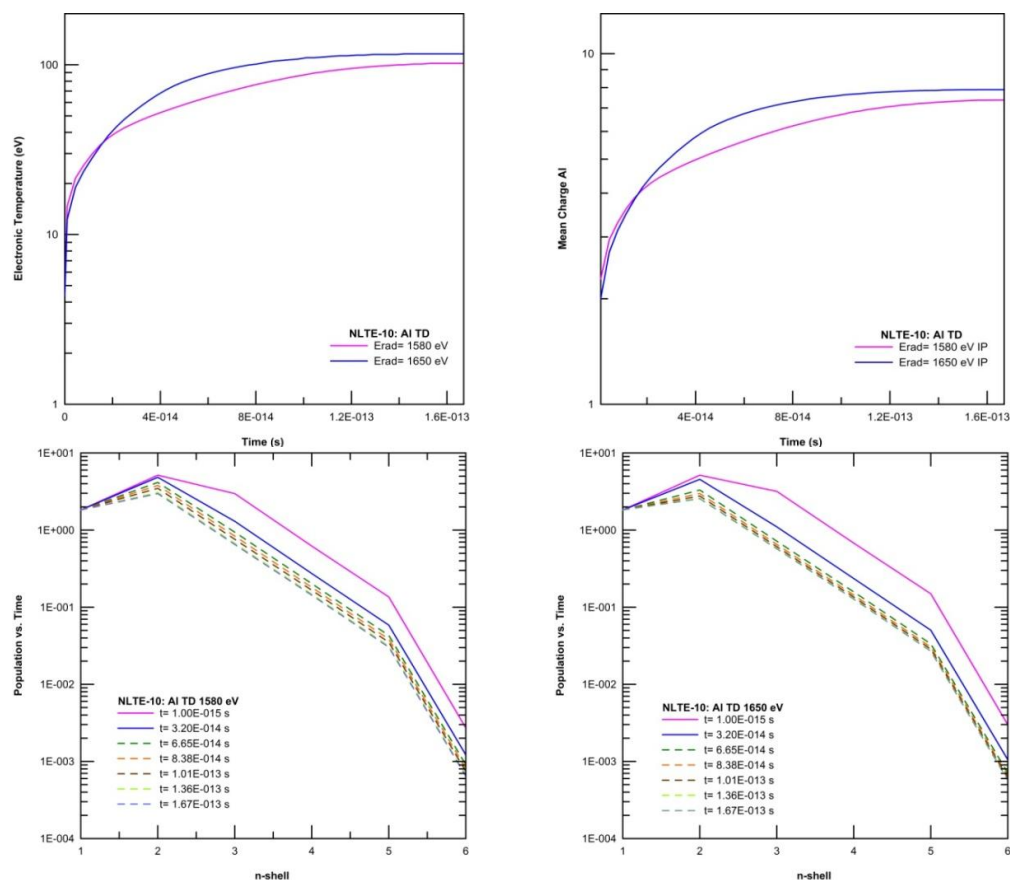


Fig. 4.a. Calculations with ATMED CR of temporal aluminium plasmas proposed in the 10th Non-LTE Code Comparison Workshop, from left to right, from upper to below graphs: electronic temperature temporal profile $T_e(t)$ of the experiments at X-ray free electron laser facilities as LCLS [11]; mean charge temporal evolution $Z_{bar}(t)$; n-shell populations temporal evolution $P_n(t)$ at $E_{rad}=1580$ or 1650 eV.

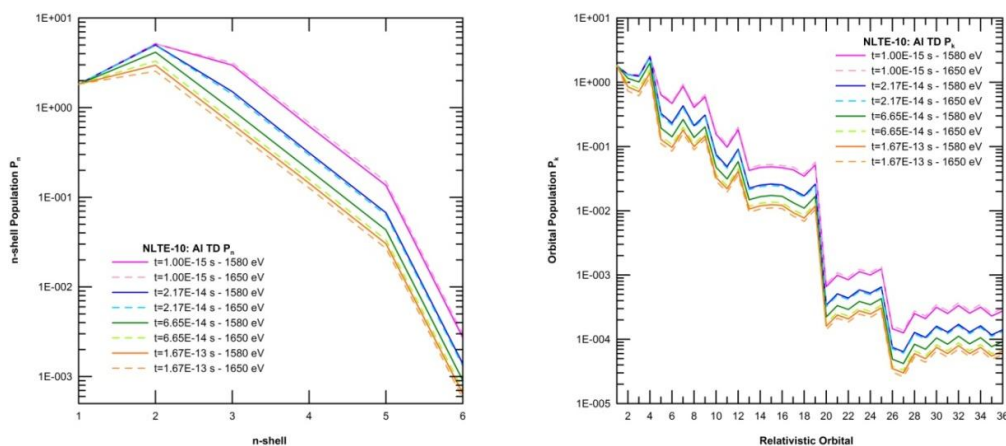


Fig. 4.b. Calculations with the code ATMED CR of temporal aluminium plasmas proposed in the 10th Non-LTE Code Comparison Workshop, from left to right graphs: n-shell populations temporal evolution $P_n(t)$ at $E_{rad}=1580$ eV versus 1650 eV and relativistic nij -shell populations temporal evolution $P_k(t)$ at $E_{rad}=1580$ eV versus 1650 eV for representative temporal intervals.

Table 2. Main populations at $t=1.67E-13$ s of thin plasmas of aluminium proposed in workshop NLTE-10

E_{rad} (eV)	$1s_{1/2}$	$2s_{1/2}$	$2p_{1/2}$	$2p_{3/2}$	$P_{n=3}$	$P_{n=4}$	$P_{n=5}$	$P_{n=6}$
1580	1.825417E+00	0.849210	0.716223	1.407132	6.522302E-01	1.434465E-01	3.037351E-02	6.435457E-04
1650	1.825415E+00	0.730117	0.615467	1.208966	5.725238E-01	1.270181E-01	2.690932E-02	5.723725E-04

Table 3. Main populations of thin plasmas of aluminium proposed in workshop NLTE-10

Time (s)	1580 eV $P_{n=1}$	1650 eV $P_{n=1}$	1580 eV $P_{n=2}$	1650 eV $P_{n=2}$	1580 eV $P_{n=3}$	1650 eV $P_{n=3}$	1580 eV $P_{n=4}$	1650 eV $P_{n=4}$
1.00E-15	1.825417E+00	1.825417E+00	5.161458E+00	5.161535E+00	2.976335E+00	3.177968E+00	6.208020E-01	6.788953E-01
1.14E-14	1.825417E+00	1.825417E+00	5.129193E+00	5.138753E+00	1.951406E+00	2.039286E+00	3.971122E-01	4.138258E-01
2.17E-14	1.825417E+00	1.825417E+00	5.000813E+00	4.939649E+00	1.509308E+00	1.415091E+00	3.139492E-01	2.964275E-01
4.58E-14	1.825417E+00	1.825417E+00	4.585584E+00	3.933569E+00	1.121546E+00	8.722511E-01	2.390337E-01	1.893481E-01
6.65E-14	1.825417E+00	1.825417E+00	4.153567E+00	3.309992E+00	9.402924E-01	7.194082E-01	2.027428E-01	1.580863E-01
9.41E-14	1.825417E+00	1.825416E+00	3.602444E+00	2.845981E+00	7.863721E-01	6.263200E-01	1.716627E-01	1.384224E-01
1.67E-13	1.825417E+00	1.825415E+00	2.972565E+00	2.554627E+00	6.522302E-01	5.725342E-01	1.434465E-01	1.270210E-01

Table 4. Main rates out of all energy levels of XFEL experiments of optically thin temporal plasmas at specific instants of neon and aluminium versus steady state plasmas, all of them proposed in the workshop NLTE-10

Rate Out (s^{-1})	Al SS $T_e=100$	Al TD $T_e=101$	Ne SS $T_e=100$	Ne TD $T_e=111$	Al SS $T_e=30$	Al TD $T_e=33.1$	Ne SS $T_e=500$	Ne TD $T_e=501$
SE	2.543149E+13	0.000000E+00	4.704842E+13	0.000000E+00	2.551392E+11	0.000000E+00	5.505854E+13	0.000000E+00
AU/DC	6.676898E+15	3.851849E+18	1.605952E+14	4.080218E+17	1.141030E+15	5.765378E+18	2.255761E+14	3.369798E+17
CE/CD	2.163898E+18	3.838387E+18	1.560524E+16	1.477701E+16	4.694591E+18	4.859419E+18	8.039752E+15	5.782858E+15
ION	4.433673E+16	1.352411E+17	2.346928E+12	3.543716E+12	4.653391E+17	4.655064E+17	2.653032E+12	1.800585E+12

SE: Spontaneous Emission; AU/DC: Autoionization/Dielectronic Capture; CE/CD: Collisional Excitation/Coll. Deexcitation; ION: Collisional Ionization; SS: Steady State; TD: Time Dependent.

Table 5. Main rates into all energy levels of XFEL experiments of optically thin temporal plasmas at specific instants of neon and aluminium versus steady state plasmas, all of them proposed in the workshop NLTE-10

Rate Into (s^{-1})	Al SS $T_e=100$	Al TD $T_e=101$	Ne SS $T_e=100$	Ne TD $T_e=111$	Al SS $T_e=30$	Al TD $T_e=33.1$	Ne SS $T_e=500$	Ne TD $T_e=501$
SE	2.696105E+14	0.000000E+00	1.202017E+12	0.000000E+00	4.448740E+14	0.000000E+00	5.996547E+11	0.000000E+00
AU/DC	1.040418E+15	1.092236E+19	8.096168E+10	2.314512E+17	5.231094E+15	9.558129E+20	4.043700E+10	1.468857E+14
CE/CD	1.618310E+17	5.610937E+17	3.208966E+11	3.201647E+12	1.926651E+18	1.989786E+18	2.368778E+11	4.339970E+11
3BREC	2.049531E+15	1.291377E+16	5.341687E+06	3.663293E+06	1.264383E+17	1.254563E+17	4.212798E+05	2.530787E+05

3BREC: 3-Body Recombination.

We can observe also in Fig. 4.b, that n-shell populations temporal evolution $P_n(t)$ at $E_{rad}=1580$ eV versus 1650 eV or $P_{nlj}(t)$ relativistic ones, follows perfectly the changes in the electronic temperature temporal profiles. See in Table 3 with more detail the populations for several instants $P_n(t)$.

More data computed with ATMED CR are collected in APPENDIX B and APPENDIX C. Sum of rates can be computed per relativistic orbital and per temporal interval, see as examples Tables C.1 and C.2 of APPENDIX C.

2.3 Relevant Highlighted Results

For the first time we have simulated plasmas created in X-rays Free Electron Laser experiments with ATMED CR, considering the electronic temperature profiles provided by the Linac Coherent Light Source (LCLS) facility. Summarizing, in the calculations that have been performed we can observe these specific remarks [16]:

1. High sensitivity to time step variations and to slight differences in radiation energies and temporal electronic temperature profiles, because of the relativistic nlj -splitting of matter atomic structure.
2. Good resolution for the order of magnitude of characteristic times of atomic processes versus characteristic time of XFEL's experiments ($E-13 \div E-15$ s), see Tables 4-5 and Figure 5. Autoionization and dielectronic capture rates ($E-16 \div E-18$ s \rightarrow $E+16 \div E+18$ s $^{-1}$) are the dominant processes in XFEL's experiments, causing an extremely rapid ionization and leaving very few electrons in the inner orbitals (full or half occupied shells in Ne 1s & in Al 1s, 2s, 2p) and the bulk of electrons in the continuum as free electrons.
3. Perfect evolution of populations $P_n(t)$ & $P_{nlj}(t)$ according to temporal profiles of electronic temperatures.
4. The evolution of mean charge follows perfectly the evolution of electronic temperature because of the high sensitivity to slight variations due to the nlj -splitting. Besides, the gaps between n-shell, nlj -shells or nlj -orbitals populations reproduce also the gaps between mean charges for specific instants.
5. ATMED CR considers all possible combination between three orbitals for

computing Autoionization and Dielectronic Capture rates, so the results of the collisional radiative balance for parameters are nearer the results of detailed models with a very complete selection of configurations and ionic charge states [2,17].

6. Absence of spontaneous emission in temporal plasmas during the whole experiment duration. This process needs more time to occur because of lifetime of excited energy levels and the stripping of electrons from energy orbitals is extremely rapid. By contrast, in steady state for Al or Ne plasmas of similar electronic density N_e and temperature T_e proposed also in the NLTE-10 Workshop, spontaneous emission takes place and has a characteristic time of $E-11 \div E-10$ s greater than the characteristic time of the experiment in the XFEL facility ($E-14 \div E-13$ s), see Tables 4-5 and Fig. 5.

The aforementioned remarks are a direct consequence of AMTED CR code being capable of computing fine grids of collisional radiative calculation for a great quantity of points inside a range not too much wide, see section 6.8 of thesis book [2]. The software is robust and sensitive to very small jumps of 2 eV in electronic temperature and of 0.25 cm^{-3} in electronic density or even smaller, without producing the typical problems that sometimes appear in the operation of a FORTRAN code (NaN, +Infinity, etc.).

This degree of resolution in the thermodynamic variables is due to the relativistic splitting of the atomic structure and can be appreciated in the evolution of plasma parameters calculated for example in the experiments of XFEL, see APPENDIXES A, B, C where it is checked that with slight jumps in time of electronic temperature $T_e(t)$ results are very exact computing without FORTRAN errors. See also Tables 4-5, APPENDIX C and Fig. 5 for comparison of properties of temporal plasmas versus steady state calculations. In Fig. 5.a it can be also checked that evolution of collisional radiative rates is as it must be in a balance calculation. For example, as density increases the collisional and three-body processes gain in importance with respect to spontaneous emission in steady state plasmas, because the number of particles inside the plasma is higher.

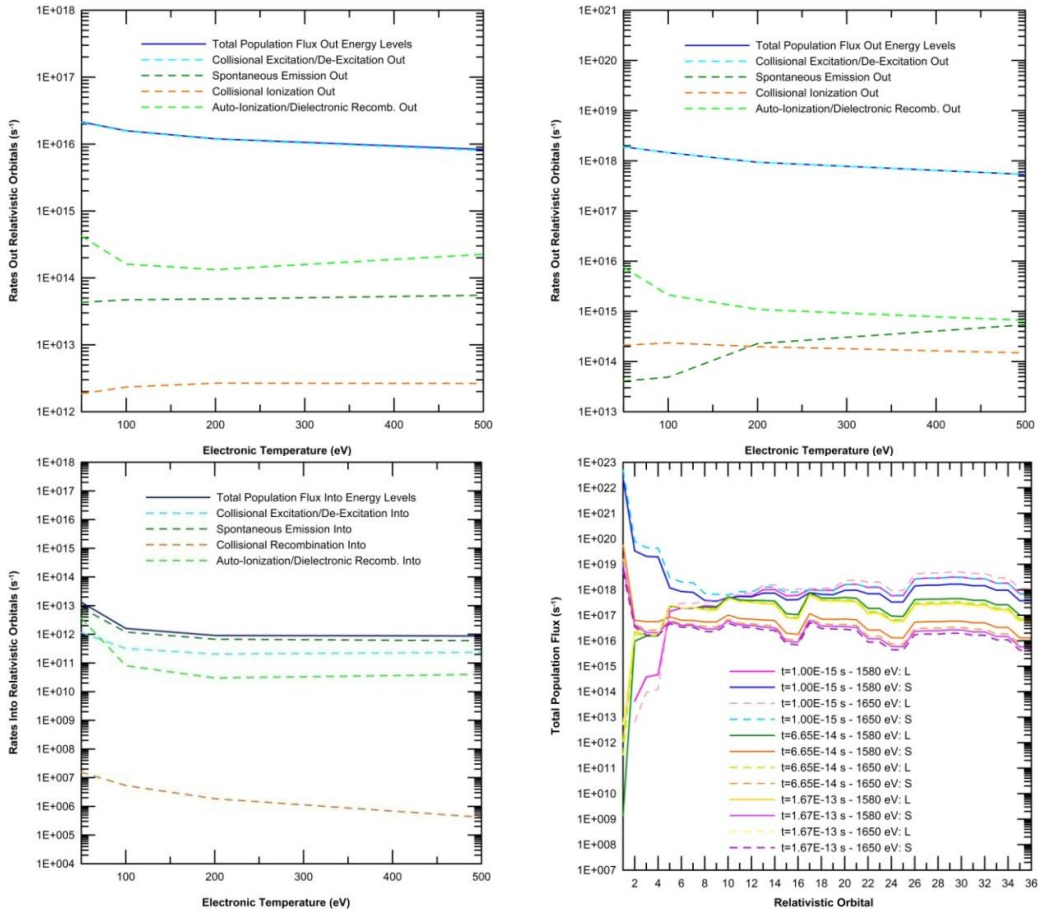


Fig. 5.a. Calculations with ATMED CR of Workshop NLTE-10, from left to right, upper to lower graphs: total depopulation rates for steady-state neon vs. electronic temperature at $N_e=1E+19 \text{ cm}^{-3}$; at $N_e=1E+21 \text{ cm}^{-3}$; total population rates for steady-state Ne at $N_e=1E+19 \text{ cm}^{-3}$ and total population (S) or depopulation (L) fluxes for aluminium per relativistic orbital for temporal intervals at $E_{\text{rad}}=1580 / 1650 \text{ eV}$

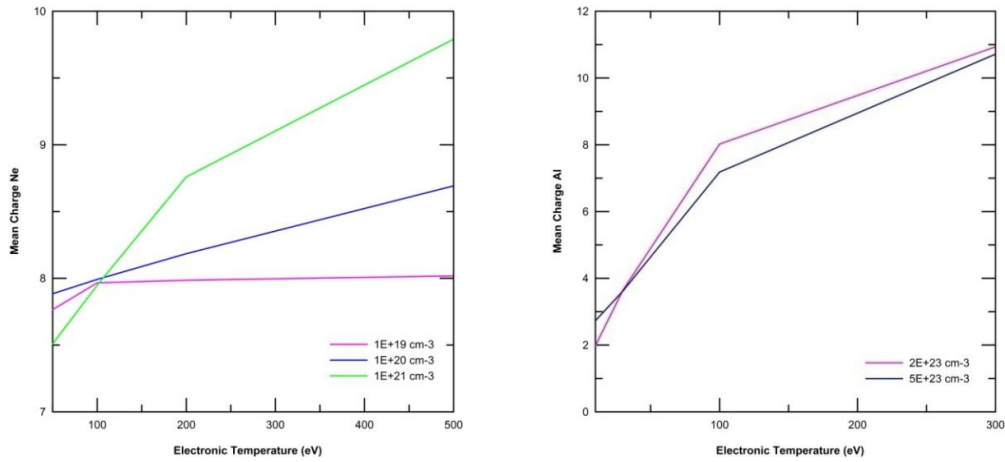


Fig. 5.b. Calculations of mean charge versus electronic temperature at several electronic densities with the code ATMED CR of steady state neon and aluminium plasmas proposed in the 10th Non-LTE Code Comparison Workshop

3. RESULTS ACCURACY OF ATMED CR CODE

In this section it is explained how in the development of this CR average atom code, a systematic, monitored, empiric and critical scientific investigation has been carried out. The typical activities specified by the Scientific Method have been performed as in Fig. 6, checking in an arranged, rigorous and well documented way the rightness of the investigation idea and definitely, the approval of the initial hypothesis being that the relativistic screened hydrogenic atomic model released in 2011 [6] and used inside the balance with atomic processes rates of ATMED CR code, would provide correct results related to plasma properties.

The Fig. 6 displays ten phases of the scientific investigation project for ATMED CR code development, culminating with the diffusion of calculated results.

1. The main idea or topic of investigation has consisted in widening the range of validity of ATMED code for computing plasmas in more conditions added to the Local Thermodynamic Equilibrium (LTE) regime.
2. The code ATMED LTE released in 2011 only allowed calculating plasmas in LTE regime so its range of validity was very narrow. In real and computational experiments it is necessary to consider common conditions of other regimes as coronal equilibrium and Non-Local Thermodynamic Equilibrium (NLTE), denominated also Collisional Radiative (CR) equilibrium.
3. The theory frame corresponds to the matter structure treatment according to Quantum Mechanics discipline, plasmas and high energy density physics and specifically atomic physics, as well as the thermodynamic and hydrodynamic analysis of laser irradiated and compressed matter. A number of 398 references have been included in the thesis book, the bulk of them have been read completely.
4. The investigation scope is delimited by the development of a model which must provide results reproducing experimental and computational values of other collisional radiative codes, similar or more

sophisticated, within previously established margins or allowed ranges.

5. The hypothesis has been to consider that the relativistic screened hydrogenic atomic model released in 2011 [6] and used inside a collisional radiative balance of an average atom, provides correct results related to plasma properties. As a consequence, the studied variables have been the atomic, radiative and thermodynamic properties of plasmas of pure elements and mixtures.
6. The investigation design has consisted of developing the software application in FORTRAN 95 programming language, being based also on iterative mathematical procedures for the CR balance resolution which speed up calculations and of standard complexity, as in Fig. 7. The data treatment and analysis have consisted of contrasting carefully results with the ones well documented in scientific bibliography and of analyzing discrepancies, detecting errors and correcting formulas, or looking for alternative formulas, until the process of testing a big enough number of plasmas of low, intermediate and high atomic number Z , has provided computed correct values in both qualitative and quantitative ways, also keeping coherence in the order of magnitude. The first version of ATMED CR code was elaborated in 2012, but the final version of 2017 has been released after comparing calculations of plasma parameters within more than 380 references.
7. Performing a gross calculation and adjusting formulas for very high temperatures, ATMED CR can model millions of plasmas of pure elements and of multiple combinations of fractions of elements in mixtures, for each value of electronic temperature T_e (eV) subdividing the logarithmic decades of input parameters within very narrow ranges, as in Fig. 8.
For example, in real experiments for measuring transmissions of Fe+Mg or Al+Fe+Mg samples with averaged values of $T_e = 195$ eV and $N_e = 8.0E+22$ cm⁻³, it is used for the correct inference of electronic temperature and density a database which contains 61 points of T_e within the range 140+250 eV, and 81 points of N_e within the range 5.0E+21+2.0E+23 cm⁻³. ATMED CR thesis includes sufficiently representative theoretical plasma cases and of

laboratories, optically thin or thick, photoionized or not, in all regimes and always with bibliographic data of reference

which support the good results of ATMED CR.

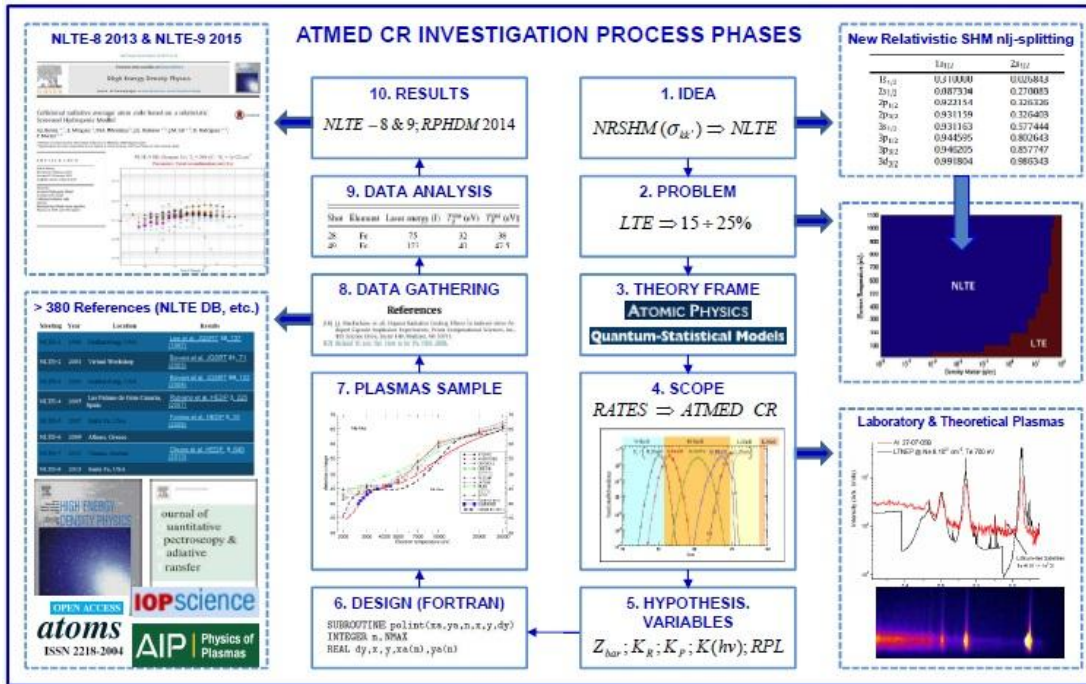


Fig. 6. Illustrative scheme of scientific investigation process for ATMED CR development

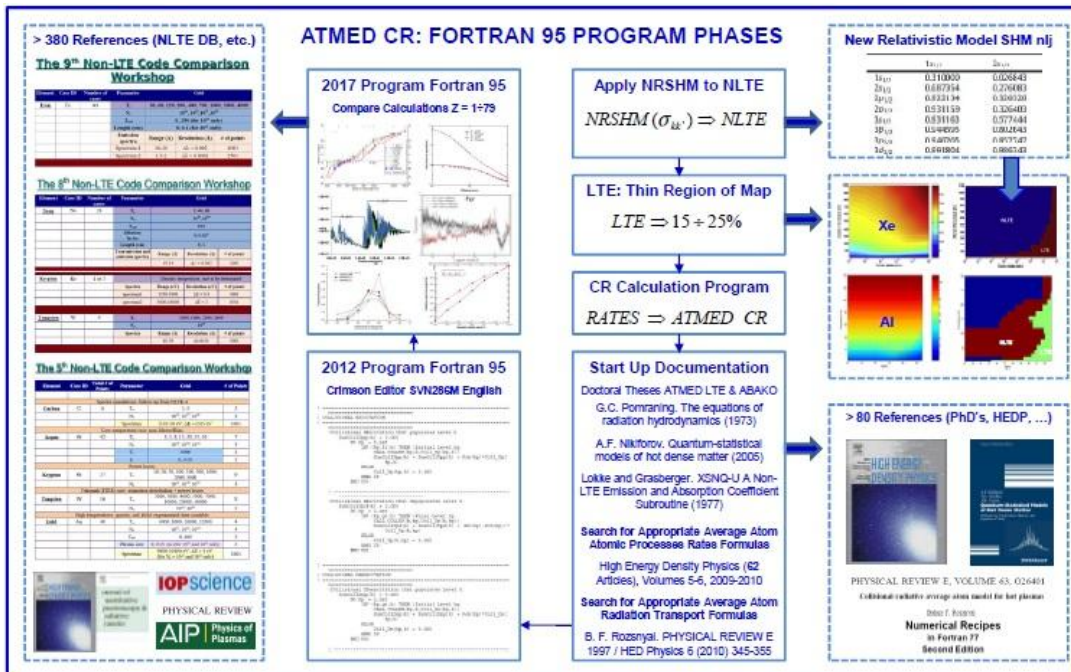


Fig. 7. Illustrative scheme of process for ATMED CR software program development

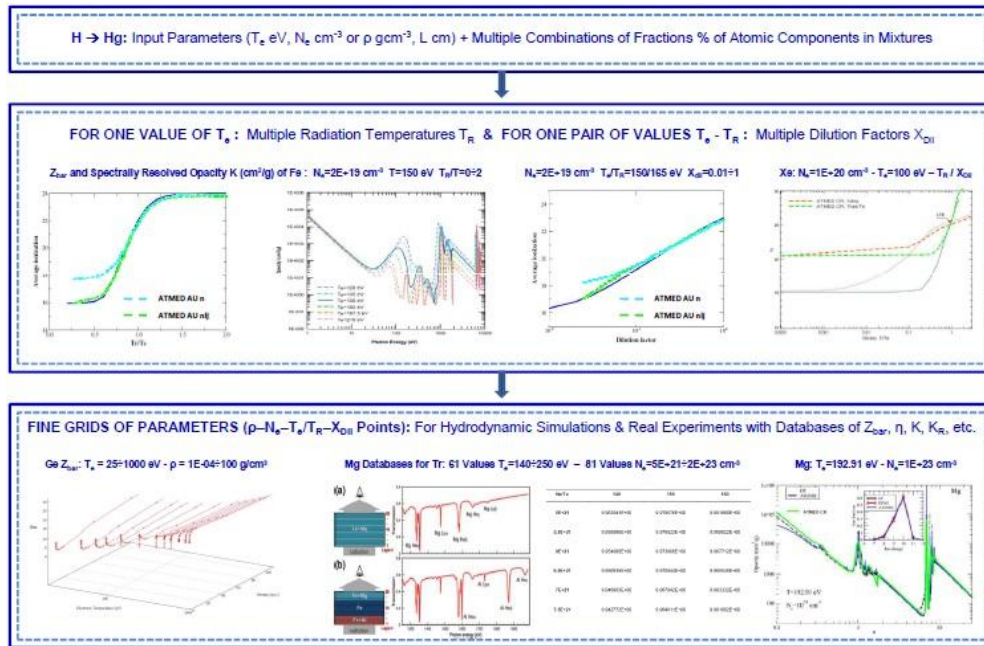


Fig. 8. Illustrative scheme of computation capability of ATMED CR: millions of plasmas

8. The data gathering process has consisted of selecting plasma cases extracted from within several books of Quantum Mechanics and Atomic Physics, doctoral theses and scientific articles, as well as from within databases generated for the specific meetings of this science area (NLTE Code Comparison and Radiative Properties of Hot Dense Matter Workshops). All the references have been useful direct or indirectly for performing the selection of plasma simulations, as well as for visualizing some applications of ATMED CR code, and finally also as a theoretical and experimental support of the written content of the doctoral thesis.
 - The 8th NLTE Code Comparison Workshop (<http://nlte.nist.gov/NLTE8/>) November 4-8, 2013, Santa Fe, NM, USA.
 - 16th International Workshop on Radiative Properties of Hot Dense Matter (RPHDM 2014), 29 Sep - 03 Oct, 2014, Vienna, Austria, EUROPE.
 - Collisional radiative average atom code based on a relativistic Screened Hydrogenic Model. A.J. Benita et al. High Energy Density Physics 14 (2015) 18-29.
 - The 9th NLTE Code Comparison Workshop (<http://nlte.nist.gov/NLTE9/>) November 30 - December 4, 2015, Paris, EUROPE.
 - The 10th NLTE Code Comparison Workshop (<http://nlte.nist.gov/NLTE10/>) November 28 - December 1 2017, San Diego, CA, USA.
9. It has been carried out a parametric analysis of data considering the most important properties which characterize plasmas, extracting the main conclusions and highlighting specific aspects of the calculation program ATMED CR.
10. Apart from including some of the most representative results inside the written thesis book [2], part of them have been also disseminated in journals of high prestige and international conferences or workshop meeting type, detailed by chronological order as follows:

Summarizing, ATMED CR provides qualitative and quantitative correct results for plasma parameters as mean charge, chemical potential, atomic processes rates, Rosseland and Planck mean opacities, Radiative Power Losses, within previously established margins by experimental measurements or computational experiments. ATMED CR spectrums of frequency resolved

opacity or transmission when superimposed on spectra of detailed codes or of other average atom codes, give way to a high agreement with respect to the averaged profile characteristics as well as to the overlapping of peaks of main electronic transition lines in UTA (Unresolved Transition Array) or MUTA (Mixed UTA) formalisms [2].

3.1 Application of ATMED CR to Other Real Temporal Experiments

Following, there are displayed calculations of ATMED CR code of temporal evolution of plasma mean charge in real experiments for comparison with simulations of other codes. The first experiment corresponds to understanding

plasma formation created irradiating aluminium planar solid targets by laser pulses of several nanoseconds. The simulations of various layers of Al slabs were performed with the one dimensional hydrocode LASNEX [18], founding Al plasmas at $T_e \sim 1000$ eV and electronic density $N_e \sim 10^{21} \text{ cm}^{-3}$, see Fig. 9.

The simulations with ATMED CR temporal module for mean charge are displayed in Fig. 10 in high agreement with Fig. 9 of Ref. [18] considering similar profiles of $T_e(t)$ and $N_e(t)$ as input data for computation. Main data of parameters evolution used in calculations of representative instants are tabulated as follows in Table 6.

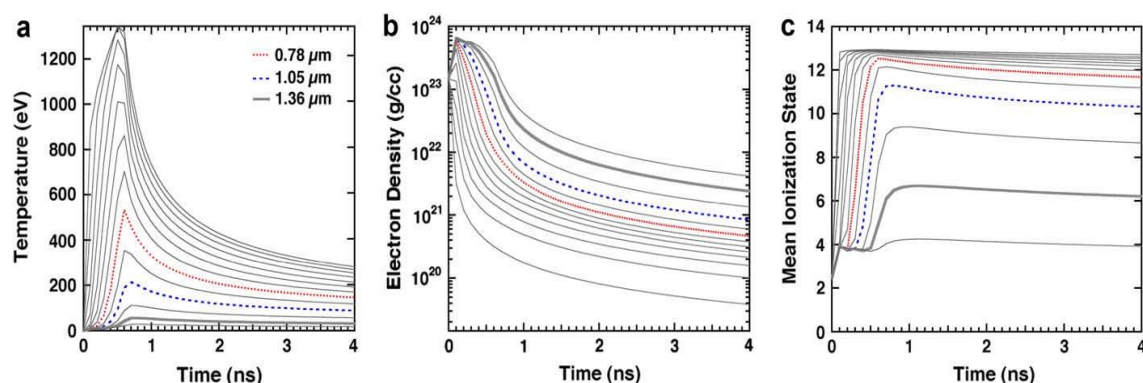


Fig. 9. Temporal evolutions of electronic temperature, density, mean charge of LASNEX of irradiated Al slabs at 0.78, 1.05, 1.36 μm [18]

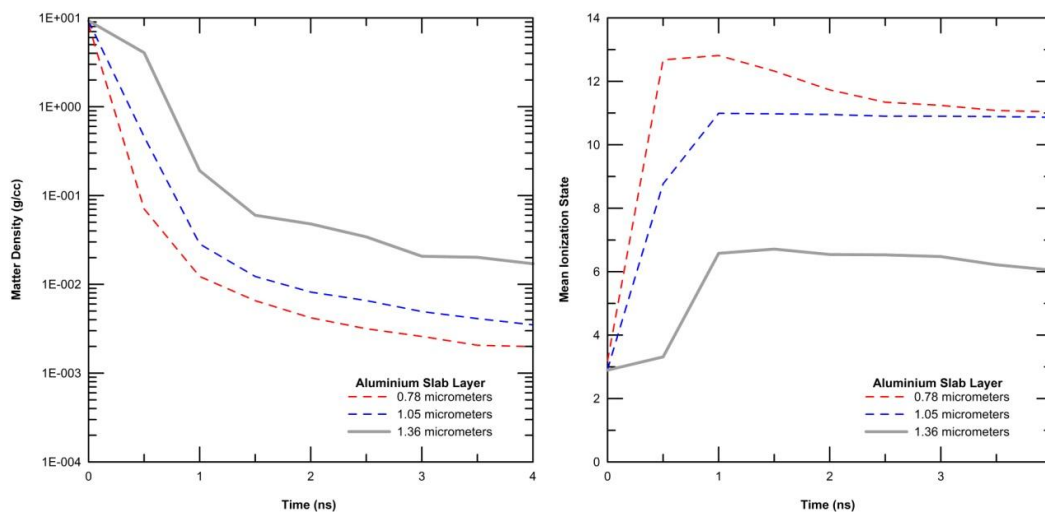


Fig. 10. Temporal evolutions of matter density and mean charge with ATMED CR of irradiated Al at layers 0.78, 1.05 and 1.36 μm [18]

Table 6. Plasma parameters for several instants with ATMED CR for similar profiles $T_e(t)$ and $N_e(t)$ to Ref. [18] with time step $\Delta t=0.5e-9$ s

Time Nanoseconds	0 ns	0.5 ns	1 ns	1.5 ns	2 ns	2.5 ns	3 ns	3.5 ns	4 ns
T_e eV (0.78 μm)	20	380	330	252	210	185	176	157	148
N_e cm^{-3} (0.78 μm)	6.0E+23	2.0E+22	3.5E+21	1.8E+21	1.1E+21	8.0E+20	6.5E+20	5.1E+20	4.9E+20
ρ g/cm^3 (0.78 μm)	8.414818	0.070672	0.012236	0.006544	0.004201	0.003160	0.002590	0.002062	0.001989
Z_{bar} (0.78 μm)	3.194661	12.679439	12.815652	12.323822	11.731208	11.342820	11.243538	11.081777	11.039411
T_e eV (1.05 μm)	10	100	171	143	124	105	100	95	90
N_e cm^{-3} (1.05 μm)	6.0E+23	9.0E+22	7.0E+21	3.0E+21	2.0E+21	1.6E+21	1.2E+21	1.0E+21	8.5E+20
ρ g/cm^3 (1.05 μm)	9.206892	0.459740	0.028528	0.012245	0.008178	0.006575	0.004931	0.004115	0.003504
Z_{bar} (1.05 μm)	2.919778	8.770972	10.993575	10.976645	10.956783	10.902072	10.902430	10.889061	10.868322
T_e eV (1.36 μm)	5	26	53	46	43	41	38	36	34
N_e cm^{-3} (1.36 μm)	6.0E+23	3.0E+23	2.8E+22	9.0E+21	7.0E+21	5.0E+21	3.0E+21	2.8E+21	2.3E+21
ρ g/cm^3 (1.36 μm)	9.286265	4.056561	0.190669	0.060072	0.047932	0.034305	0.020752	0.020182	0.017044
Z_{bar} (1.36 μm)	2.894869	3.313414	6.579481	6.712576	6.543249	6.530147	6.476949	6.215954	6.046191

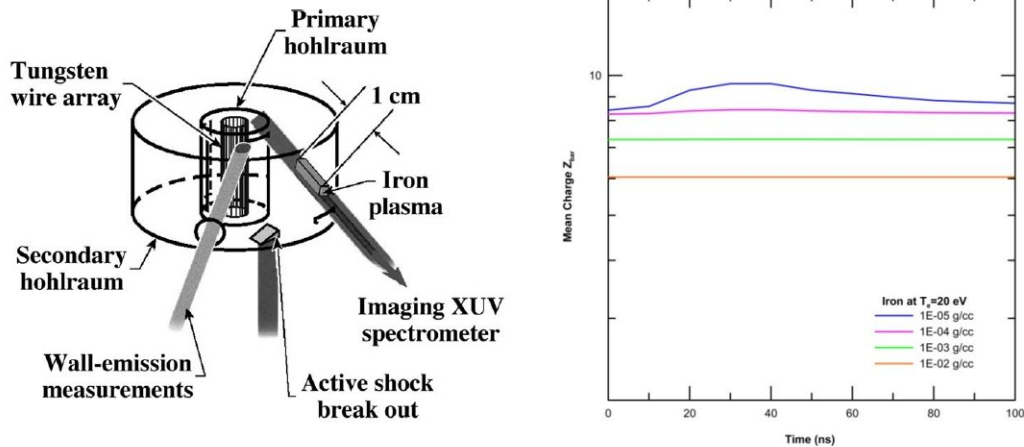


Fig. 11. Temporal evolutions of mean charge with ATMED CR of iron samples at Saturn facility [19,20]

The second experiment corresponds to measuring in pulsed power Saturn facility, relevant opacity data in astrophysics of pulsating stars “Cepheids” which correspond to variable envelopes, belonging to temperatures of 20 eV and equivalent densities in iron of the order of $1\text{E-}04\text{ g/cm}^3$ [19,20]. It is generated a variable radiation temperature $T_R(t)$ with time with a peak of 70 eV. Through a dispositive, it is adjusted the energy flux to get the desired radiation temperature of 20 eV as seen by the sample target composed of $\text{FeO}_{0.41}$ tamped with $\text{C}_{16}\text{H}_{14}\text{O}_{1.68}$, reaching a regime of local thermodynamic equilibrium for the measurement. The simulations with ATMED CR for iron mean charge with a less oscillating evolution of values are displayed in Fig. 11, in high agreement with Fig. 4 of Ref. [18] and also at several densities, electronic temperature $T_e = 20\text{ eV}$ and according to the temporal profile of the radiation temperature generated in the experiment (Fig. 8 of Ref. [18]). At matter density $1\text{E-}05\text{ g/cm}^3$ the evolution of mean charge is even more exact with ATMED CR following better the profile of $T_R(t)$, and for higher densities in the range $\rho = 1\text{E-}04\text{--}1\text{E-}02\text{ g/cm}^3$ the evolution of Z_{bar} depends more strongly on the electronic temperature without greater variations with time.

More data are collected in Ref. [2] for both experiments and considering very similar temporal profiles for the evolution of thermodynamic variables.

4. SUMMARY AND CONCLUSIONS

In this paper, we model with ATMED CR neon and aluminium temporal plasmas, proposed in

the 10th Non-LTE Code Comparison Workshop [11,16] of interest for the study of laser-matter interaction in X-rays free electron laser facilities. XFEL is a marvelous laser enabling atomic level analysis which requires a kilometer order accelerator being used for diagnosis and life-extension of structures or advanced medical solutions within other science applications. It generates ultrashort and extremely bright X-ray flashes for studies in disciplines like physics, chemistry, life sciences, and materials research.

The results for plasma properties can be considered as very precise, according to the electronic temperature profiles registered in experiments of laser created plasmas with duration times of picoseconds and femtoseconds. The Crank-Nicholson implicit numerical iterative method implemented inside the temporal module of ATMED CR without matricial resolution, is very rapid and useful for calculating statistical averaged plasma properties for this type of experiments, avoiding some of the typical difficulties encountered when interpreting the simulation of plasmas created with free electron lasers [13] as for example, very different temporal scales in Non Local Thermodynamic Equilibrium regime, enormous matrices of detailed collisional radiative codes, etc. Considering the duration times of experiments in comparison with characteristic times of the atomic processes rates, the calculations are very accurate because the collisional radiative balance of ATMED CR is a statistical average of the results of detailed models, even for durations of laser irradiation of picoseconds and femtoseconds.

COMPETING INTERESTS

Author has declared that no competing interests exist.

REFERENCES

1. Benita AJ, Mínguez E, Mendoza MA, Rubiano JG, Gil JM, Rodríguez R, Martel P. Collisional radiative average atom code based on a relativistic screened hydrogenic model. *High Energy Density Physics*. 2015;14:18-29.
2. Benita AJ. Collisional radiative average atom code with relativistic atomic model. *Theoretical physics*. ISBN: 978-620-2-01943-9. LAP Lambert Academic Publishing; 2017.
3. Benita AJ. Fast calculation of plasmas properties with ATMED LTE. Project of Nuclear Science and Technology Master at UPM; 2012.
4. Mendoza MA, Rubiano JG, Gil JM, Rodríguez R, Florido R, Benita AJ, Martel P, Mínguez E. Fast computation of radiative properties and EOS of warm dense matter using the ATMED code. Eight International Conference on Inertial Fusion Sciences and Applications (IFSA 2013). September 8 -13 (2013) Nara, Japan.
5. Mendoza MA, Rubiano JG, Gil JM, Rodríguez R, Florido R, Espinosa G, Martel P, Mínguez E. Calculation of radiative opacity of plasma mixtures using a relativistic screened hydrogenic model. *Journal of Quantitative Spectroscopy & Radiative Transfer*. 2014;140:81–98.
6. Mendoza MA, Rubiano JG, Gil JM, Rodríguez R, Florido R, Martel P, Mínguez E. A new set of relativistic screening constants for the screened hydrogenic model. *HEDP*. 2011;7:169–179.
7. Ruano FH, Rubiano JG, Mendoza MA, Gil JM, Rodríguez R, Florido R, Martel P, Mínguez E. Relativistic screened hydrogenic radial integrals. *Journal of Quantitative Spectroscopy & Radiative Transfer*. 2012;117:123-132.
8. Lokke WA, Grasberger WH. XSNQ-U A Non-LTE emission and absorption coefficient subroutine. Prepared for U.S. Energy Research & Development Administration under contract No. W-7405-Eng-48, UCRL-52276; 1977.
9. Faussurier G, Blancard C, Kato T, More RM. Prigogine theorem of minimum entropy production applied to the average atom model. *High Energy Density Physics*. 2009;5:283.
10. Balazs F, Rozsnyai. Collisional radiative average atom model for hot plasmas. *Physical Review E*. 1996;55.
11. The 10th NLTE Code Comparison Workshop. November 28 - December 1 2017, San Diego, CA, USA. Available:<http://nlte.nist.gov/NLTE10/>
12. Faussurier G, et al. Non local thermodynamic equilibrium self-consistent average atom model for plasma physics. *Physical Review E*. 2001;63, 026401.
13. Riconda C, Weber S. Interaction Rayonnement-Plasmas: de la FCI au XFEL, outils et projets au sein du LULI/PAPD. Journée Plasmas, Université Pierre et Marie Curie (UPMC), Paris; 2008.
14. Young L, et al. Femtosecond electronic response of atoms to ultra-intense X-rays. *Nature*. 2010;466. DOI: 10.1038/nature09177
15. Ciricosta O, et al. Direct measurements of the ionization potential depression in a dense plasma; 2012. DOI: 10.1103/PhysRevLett.109.065002
16. Benita AJ. The 10th NLTE Code Comparison Workshop. Available:https://www.researchgate.net/profile/Aj_Benita
17. Wu ZQ, Duan B, Yan J. Effects of different doubly excited states on the ionization balance and M-emissivity in high-Z plasmas. *High Energy Density Physics*. 2014;11:70–74.
18. Chung HK, Lee RW. Applications of NLTE population kinetics. *High Energy Density Physics*. 2009;5:1–14.
19. Springer PT, et al. Laboratory measurement of opacity for stellar envelopes. *Journal of Quantitative Spectroscopy Radiative Transfer*. 1997;58(4-6):927-935.
20. Bruce A. Remington, et al. Experimental astrophysics with high power lasers and Z pinches. *Reviews of Modern Physics*. 2006;78.

APPENDIX A. Properties of Neon Plasmas of XFEL Experiments

Table A.1. Evolution of plasma parameters depending on the characteristics of the experiment with ATMED CR and considering plasma effects with ionization pressure (IP) mode similar to Ecker-Kröll model or continuum lowering (CL) mode with formulas of Stewart-Pyatt.

Time (s)	$E_{\text{rad}}=800$ eV T_e (eV)	$E_{\text{rad}}=800$ eV Z_{bar} IP	$E_{\text{rad}}=1050$ eV T_e (eV)	$E_{\text{rad}}=1050$ eV Z_{bar} IP	$E_{\text{rad}}=1050$ eV Z_{bar} CL	$E_{\text{rad}}=2000$ eV T_e (eV)	$E_{\text{rad}}=2000$ eV Z_{bar} IP	$E_{\text{rad}}=2000$ eV Z_{bar} CL	Time Step (s)
3.70E-14	54.1	4.994	102.0	6.634	6.822	10.6	4.090	4.133	9.0E-15
4.60E-14	67.8	5.249	123.0	6.772	6.981	14.1	4.157	4.257	9.0E-15
5.49E-14	82.1	5.505	143.0	6.928	7.152	18.2	4.303	4.491	8.9E-15
6.39E-14	96.7	5.755	163.0	7.107	7.337	23.1	4.503	4.765	9.0E-15
7.29E-14	112.0	5.996	181.0	7.296	7.531	29.7	4.727	5.059	9.0E-15
8.19E-14	126.0	6.229	196.0	7.486	7.708	38.7	4.960	5.368	9.0E-15
9.09E-14	141.0	6.461	208.0	7.657	7.851	49.9	5.194	5.692	9.0E-15
9.99E-14	156.0	6.695	218.0	7.803	7.960	63.0	5.439	5.999	9.0E-15
1.09E-13	172.0	6.935	226.0	7.913	8.044	77.7	5.682	6.266	9.1E-15
1.18E-13	188.0	7.174	232.0	7.996	8.111	93.8	5.912	6.497	9.0E-15
1.27E-13	203.0	7.402	237.0	8.061	8.168	111.0	6.130	6.690	9.0E-15
1.36E-13	219.0	7.611	241.0	8.114	8.219	130.0	6.352	6.884	9.0E-15
1.45E-13	234.0	7.785	244.0	8.159	8.265	151.0	6.588	7.092	9.0E-15
1.54E-13	248.0	7.919	246.0	8.200	8.308	175.0	6.858	7.322	9.0E-15
1.63E-13	262.0	8.021	249.0	8.238	8.347	201.0	7.149	7.564	9.0E-15
1.72E-13	275.0	8.101	250.0	8.272	8.384	228.0	7.436	7.779	9.0E-15
1.81E-13	287.0	8.168	252.0	8.305	8.419	255.0	7.687	7.947	9.0E-15
1.90E-13	298.0	8.229	253.0	8.335	8.452	280.0	7.879	8.076	9.0E-15
1.99E-13	308.0	8.284	255.0	8.365	8.483	306.0	8.020	8.182	9.0E-15
2.08E-13	318.0	8.336	256.0	8.392	8.513	330.0	8.127	8.275	9.0E-15
2.17E-13	327.0	8.385	257.0	8.419	8.542	354.0	8.215	8.359	9.0E-15
2.26E-13	335.0	8.431	258.0	8.444	8.569	377.0	8.292	8.437	9.0E-15
2.35E-13	343.0	8.476	259.0	8.469	8.595	397.0	8.362	8.509	9.0E-15
2.44E-13	350.0	8.518	260.0	8.492	8.620	416.0	8.426	8.576	9.0E-15
2.53E-13	356.0	8.558	261.0	8.515	8.644	433.0	8.486	8.638	9.0E-15
2.62E-13	362.0	8.596	262.0	8.537	8.667	447.0	8.541	8.696	9.0E-15
2.71E-13	367.0	8.632	263.0	8.558	8.690	461.0	8.592	8.749	9.0E-15
2.80E-13	372.0	8.667	264.0	8.578	8.712	472.0	8.640	8.799	9.0E-15
2.89E-13	376.0	8.700	265.0	8.598	8.733	483.0	8.686	8.846	9.0E-15
2.98E-13	380.0	8.732	266.0	8.618	8.753	492.0	8.728	8.890	9.0E-15
3.07E-13	383.0	8.763	267.0	8.637	8.773	501.0	8.768	8.931	9.0E-15
3.16E-13	386.0	8.792	268.0	8.655	8.793	509.0	8.806	8.970	9.0E-15

Time (s)	$E_{\text{rad}}=800$ eV T_e (eV)	$E_{\text{rad}}=800$ eV Z_{bar} IP	$E_{\text{rad}}=1050$ eV T_e (eV)	$E_{\text{rad}}=1050$ eV Z_{bar} IP	$E_{\text{rad}}=1050$ eV Z_{bar} CL	$E_{\text{rad}}=2000$ eV T_e (eV)	$E_{\text{rad}}=2000$ eV Z_{bar} IP	$E_{\text{rad}}=2000$ eV Z_{bar} CL	Time Step (s)
3.25E-13	388.0	8.820	269.0	8.673	8.812	516.0	8.842	9.006	9.0E-15
3.34E-13	391.0	8.847	270.0	8.691	8.830	523.0	8.876	9.041	9.0E-15
3.43E-13	393.0	8.873	271.0	8.708	8.848	530.0	8.908	9.073	9.0E-15
3.52E-13	394.0	8.897	272.0	8.724	8.865	537.0	8.939	9.104	9.0E-15
3.61E-13	396.0	8.921	273.0	8.741	8.882	543.0	8.968	9.134	9.0E-15
3.70E-13	397.0	8.944	274.0	8.757	8.899	550.0	8.996	9.162	9.0E-15
3.79E-13	398.0	8.966	274.0	8.772	8.915	556.0	9.023	9.189	9.0E-15
3.88E-13	399.0	8.988	275.0	8.788	8.931	562.0	9.049	9.214	9.0E-15
3.97E-13	400.0	9.008	276.0	8.803	8.947	568.0	9.073	9.238	9.0E-15
4.06E-13	401.0	9.028	277.0	8.817	8.962	573.0	9.097	9.262	9.0E-15
4.15E-13	401.0	9.047	277.0	8.832	8.977	579.0	9.120	9.284	9.0E-15
4.24E-13	402.0	9.066	278.0	8.846	8.991	584.0	9.142	9.305	9.0E-15
4.33E-13	402.0	9.084	278.0	8.860	9.005	588.0	9.163	9.326	9.0E-15
4.42E-13	402.0	9.099	279.0	8.872	9.017	592.0	9.181	9.343	9.0E-15
4.50E-13	403.0	9.116	279.0	8.885	9.031	596.0	9.201	9.362	8.0E-15
4.59E-13	403.0	9.132	279.0	8.898	9.044	600.0	9.220	9.380	9.0E-15
4.68E-13	403.0	9.148	280.0	8.910	9.057	603.0	9.238	9.398	9.0E-15
4.77E-13	403.0	9.163	280.0	8.923	9.070	605.0	9.256	9.415	9.0E-15
4.86E-13	404.0	9.178	280.0	8.935	9.082	608.0	9.273	9.431	9.0E-15
4.95E-13	404.0	9.193	281.0	8.947	9.094	610.0	9.289	9.446	9.0E-15
5.04E-13	404.0	9.207	281.0	8.958	9.106	611.0	9.305	9.461	9.0E-15
5.13E-13	404.0	9.220	281.0	8.970	9.117	613.0	9.321	9.476	9.0E-15
5.22E-13	404.0	9.234	281.0	8.981	9.129	614.0	9.336	9.490	9.0E-15
5.31E-13	404.0	9.247	282.0	8.992	9.140	616.0	9.350	9.503	9.0E-15
5.40E-13	404.0	9.259	282.0	9.003	9.151	617.0	9.364	9.516	9.0E-15
5.49E-13	404.0	9.272	282.0	9.014	9.161	617.0	9.378	9.529	9.0E-15
5.58E-13	404.0	9.284	282.0	9.024	9.172	618.0	9.391	9.541	9.0E-15
5.67E-13	404.0	9.295	282.0	9.034	9.182	619.0	9.404	9.552	9.0E-15
5.76E-13	404.0	9.307	282.0	9.044	9.192	619.0	9.416	9.564	9.0E-15
5.85E-13	404.0	9.318	282.0	9.054	9.201	619.0	9.428	9.575	9.0E-15
5.94E-13	404.0	9.328	282.0	9.063	9.211	620.0	9.440	9.585	9.0E-15
6.03E-13	404.0	9.339	282.0	9.073	9.220	620.0	9.451	9.595	9.0E-15
6.12E-13	404.0	9.349	282.0	9.082	9.229	620.0	9.462	9.605	9.0E-15
6.21E-13	404.0	9.359	282.0	9.091	9.238	620.0	9.473	9.615	9.0E-15
6.30E-13	404.0	9.369	282.0	9.100	9.247	621.0	9.484	9.624	9.0E-15
6.39E-13	404.0	9.379	282.0	9.109	9.256	621.0	9.494	9.633	9.0E-15
6.48E-13	404.0	9.388	282.0	9.118	9.264	621.0	9.504	9.642	9.0E-15

Time (s)	$E_{\text{rad}}=800 \text{ eV } T_e \text{ (eV)}$	$E_{\text{rad}}=800 \text{ eV } Z_{\text{bar}} \text{ IP}$	$E_{\text{rad}}=1050 \text{ eV } T_e \text{ (eV)}$	$E_{\text{rad}}=1050 \text{ eV } Z_{\text{bar}} \text{ IP}$	$E_{\text{rad}}=1050 \text{ eV } Z_{\text{bar}} \text{ CL}$	$E_{\text{rad}}=2000 \text{ eV } T_e \text{ (eV)}$	$E_{\text{rad}}=2000 \text{ eV } Z_{\text{bar}} \text{ IP}$	$E_{\text{rad}}=2000 \text{ eV } Z_{\text{bar}} \text{ CL}$	Time Step (s)
6.57E-13	404.0	9.397	282.0	9.126	9.273	621.0	9.514	9.651	9.0E-15
6.66E-13	404.0	9.406	282.0	9.134	9.281	621.0	9.523	9.659	9.0E-15
6.75E-13	404.0	9.415	282.0	9.143	9.289	621.0	9.532	9.667	9.0E-15
6.84E-13	404.0	9.424	282.0	9.151	9.297	621.0	9.541	9.675	9.0E-15
6.93E-13	404.0	9.432	282.0	9.159	9.304	621.0	9.550	9.682	9.0E-15
7.02E-13	404.0	9.441	282.0	9.166	9.312	621.0	9.558	9.690	9.0E-15
7.11E-13	404.0	9.449	282.0	9.174	9.319	621.0	9.567	9.697	9.0E-15
7.20E-13	404.0	9.457	282.0	9.182	9.327	621.0	9.575	9.704	9.0E-15
7.29E-13	404.0	9.464	282.0	9.189	9.334	621.0	9.583	9.710	9.0E-15
7.38E-13	404.0	9.472	282.0	9.196	9.341	621.0	9.590	9.717	9.0E-15
7.47E-13	404.0	9.479	282.0	9.203	9.348	621.0	9.598	9.723	9.0E-15
7.56E-13	404.0	9.487	282.0	9.211	9.355	621.0	9.605	9.730	9.0E-15
7.65E-13	404.0	9.494	282.0	9.218	9.362	621.0	9.613	9.736	9.0E-15
7.74E-13	404.0	9.501	282.0	9.224	9.368	621.0	9.620	9.741	9.0E-15
7.83E-13	404.0	9.508	282.0	9.231	9.375	621.0	9.627	9.747	9.0E-15
7.92E-13	404.0	9.515	282.0	9.238	9.381	621.0	9.633	9.753	9.0E-15
8.01E-13	404.0	9.521	282.0	9.245	9.388	621.0	9.640	9.758	9.0E-15
8.10E-13	404.0	9.528	282.0	9.251	9.394	621.0	9.646	9.764	9.0E-15
8.19E-13	404.0	9.534	282.0	9.257	9.400	621.0	9.652	9.769	9.0E-15
8.28E-13	404.0	9.541	282.0	9.264	9.406	621.0	9.659	9.774	9.0E-15
8.37E-13	404.0	9.547	282.0	9.270	9.412	621.0	9.665	9.779	9.0E-15
8.55E-13	404.0	9.559	282.0	9.282	9.424	621.0	9.676	9.788	9.0E-15
8.73E-13	404.0	9.570	282.0	9.294	9.435	621.0	9.687	9.797	9.0E-15
8.82E-13	404.0	9.576	282.0	9.300	9.440	621.0	9.693	9.801	9.0E-15
8.91E-13	404.0	9.582	282.0	9.306	9.446	621.0	9.698	9.806	9.0E-15

APPENDIX B. Properties of Aluminium Plasmas of XFEL Experiments

Table B.1. Evolution of plasma parameters depending on the characteristics of the experiment with ATMED CR at $N_{ion}= 6.0E+22 \text{ cm}^{-3}$

Time (s)	$E_{rad}=1580 \text{ eV } T_e \text{ (eV)}$	$E_{rad}=1580 \text{ eV } Z_{bar}$	$E_{rad}=1580 \text{ eV } N_e \text{ (cm}^{-3}\text{)}$	$E_{rad}=1650 \text{ eV } T_e \text{ (eV)}$	$E_{rad}=1650 \text{ eV } Z_{bar}$	$E_{rad}=1650 \text{ eV } N_e \text{ (cm}^{-3}\text{)}$	Time Step (s)
1.00E-15	14.7	2.277	1.366452E+23	12.3	2.003	1.202125E+23	1.00E-15
7.90E-15	25.6	3.292	1.975738E+23	23.6	3.127	1.876636E+23	3.45E-15
1.48E-14	33.7	3.877	2.326571E+23	33.1	3.834	2.300754E+23	3.40E-15
2.17E-14	40.1	4.281	2.569109E+23	43.3	4.458	2.675141E+23	3.50E-15
2.86E-14	45.0	4.572	2.743322E+23	52.6	4.980	2.988218E+23	3.50E-15
3.55E-14	49.5	4.827	2.896691E+23	62.0	5.478	3.287395E+23	3.50E-15
4.24E-14	53.7	5.061	3.036874E+23	71.2	5.939	3.563439E+23	3.50E-15
4.93E-14	57.9	5.288	3.173331E+23	79.0	6.308	3.784931E+23	3.50E-15
5.27E-14	60.0	5.401	3.240658E+23	82.3	6.462	3.877507E+23	3.40E-15
5.96E-14	64.2	5.620	3.372313E+23	88.3	6.729	4.037739E+23	3.40E-15
6.65E-14	68.4	5.833	3.500344E+23	93.3	6.952	4.171732E+23	3.40E-15
7.34E-14	72.5	6.034	3.620855E+23	97.6	7.139	4.283762E+23	3.40E-15
8.03E-14	76.6	6.228	3.737346E+23	101.0	7.288	4.373352E+23	3.40E-15
8.72E-14	80.5	6.409	3.845934E+23	105.0	7.436	4.461887E+23	3.40E-15
9.41E-14	84.2	6.576	3.946160E+23	107.0	7.533	4.520347E+23	3.40E-15
1.01E-13	87.6	6.725	4.035325E+23	110.0	7.628	4.576865E+23	3.40E-15
1.08E-13	90.7	6.865	4.119274E+23	111.0	7.687	4.612443E+23	4.00E-15
1.15E-13	93.4	6.985	4.191364E+23	113.0	7.755	4.653504E+23	4.00E-15
1.22E-13	95.7	7.087	4.252293E+23	114.0	7.798	4.679056E+23	4.00E-15
1.29E-13	97.6	7.170	4.302521E+23	115.0	7.835	4.701109E+23	4.00E-15
1.32E-13	98.4	7.209	4.325478E+23	115.0	7.848	4.708912E+23	3.00E-15
1.39E-13	99.8	7.265	4.359383E+23	115.0	7.855	4.713425E+23	3.00E-15
1.53E-13	102.0	7.353	4.412361E+23	116.0	7.891	4.734734E+23	4.00E-15

^a E_{rad} : Radiation Energy.

APPENDIX C. Atomic Processes Rates of Aluminium Plasmas of XFEL Experiments

Table C.1. Populating and depopulating rates of all orbitals for some temporal intervals representative of plasma evolution with ATMED CR of aluminium plasma with the conditions $T_e(t)$ eV, $N_{ion} = 6.0E+22 \text{ cm}^{-3}$ and $E_{rad} = 1650 \text{ eV}$

Time (s)	T_e (eV)	SE Out/Into Rate (s^{-1})	3-Body Rec. Rate (s^{-1})	Coll. Ioniz. Rate (s^{-1})	Autoloniz./DC Into Rate (s^{-1})	Autoloniz./DC Out Rate (s^{-1})	Col. De/Exc. Into Rate (s^{-1})	Col. De/Exc. Out Rate (s^{-1})
1.00E-15	12.3	0.000000E+00	1.033282E+18	1.607570E+18	5.108273E+22	5.716449E+19	3.613683E+18	3.602012E+18
7.90E-15	23.6	0.000000E+00	2.528387E+17	6.853298E+17	3.427418E+21	9.275549E+18	2.624102E+18	4.633524E+18
1.48E-14	33.1	0.000000E+00	1.254563E+17	4.655064E+17	9.558129E+20	5.765378E+18	1.989786E+18	4.859419E+18
2.17E-14	43.3	0.000000E+00	7.274133E+16	3.502816E+17	3.593232E+20	6.020609E+18	1.526383E+18	4.828971E+18
2.86E-14	52.6	0.000000E+00	4.899262E+16	2.836701E+17	1.720913E+20	6.184029E+18	1.234399E+18	4.689079E+18
3.55E-14	62.0	0.000000E+00	3.502851E+16	2.360290E+17	8.997844E+19	5.982304E+18	1.023930E+18	4.505496E+18
4.24E-14	71.2	0.000000E+00	2.640360E+16	2.018631E+17	5.125642E+19	5.538101E+18	8.718665E+17	4.322298E+18
4.93E-14	79.0	0.000000E+00	2.135610E+16	1.795217E+17	3.322006E+19	5.064169E+18	7.708337E+17	4.176763E+18
5.27E-14	82.3	0.000000E+00	1.963793E+16	1.712330E+17	2.780532E+19	4.870021E+18	7.328539E+17	4.119152E+18
5.96E-14	88.3	0.000000E+00	1.701566E+16	1.582408E+17	2.050892E+19	4.528196E+18	6.718454E+17	4.020850E+18
6.65E-14	93.3	0.000000E+00	1.519769E+16	1.484136E+17	1.593595E+19	4.254606E+18	6.251814E+17	3.944907E+18
7.34E-14	97.6	0.000000E+00	1.385836E+16	1.408892E+17	1.291762E+19	4.028711E+18	5.886710E+17	3.883977E+18
8.03E-14	101.0	0.000000E+00	1.291377E+16	1.352411E+17	1.092236E+19	3.851849E+18	5.610937E+17	3.838387E+18
8.72E-14	105.0	0.000000E+00	1.195557E+16	1.301685E+17	9.254544E+18	3.674792E+18	5.342649E+17	3.788709E+18
9.41E-14	107.0	0.000000E+00	1.148338E+16	1.267721E+17	8.290893E+18	3.563368E+18	5.180178E+17	3.764132E+18
1.01E-13	110.0	0.000000E+00	1.088764E+16	1.239122E+17	7.455531E+18	3.447342E+18	5.014567E+17	3.730383E+18
1.08E-13	111.0	0.000000E+00	1.066527E+16	1.219097E+17	6.969615E+18	3.380541E+18	4.923174E+17	3.718627E+18
1.15E-13	113.0	0.000000E+00	1.029713E+16	1.198844E+17	6.448436E+18	3.295996E+18	4.809715E+17	3.697144E+18
1.22E-13	114.0	0.000000E+00	1.011048E+16	1.185826E+17	6.142643E+18	3.246915E+18	4.742752E+17	3.686460E+18
1.29E-13	115.0	0.000000E+00	9.935098E+15	1.175109E+17	5.890366E+18	3.206288E+18	4.684080E+17	3.676089E+18
1.39E-13	115.0	0.000000E+00	9.912380E+15	1.167731E+17	5.752748E+18	3.187469E+18	4.657740E+17	3.675624E+18
1.53E-13	116.0	0.000000E+00	9.743187E+15	1.157685E+17	5.523173E+18	3.142779E+18	4.601493E+17	3.665471E+18

Col. De/Exc. Into/Out: Collisional Deexcitation/Excitation Into/Out Energy Levels; SE: Spontaneous Emission; Autoloniz./DC: Autoionization/Dielectronic Capture.

Table C.2. Populating and depopulating rates of some relativistic orbitals at temporal interval 6.65E-14 s with ATMED CR of aluminium plasma with the conditions $T_e = 93.3$ eV, $Z_{\text{bar}} = 6.952$, $N_{\text{ion}} = 6.0\text{E}+22$ cm⁻³ and $E_{\text{rad}} = 1650$ eV, spontaneous emission out/in orbitals is zero

P_k Symbol	P_k Number	Col. Exc. Into Rate (s⁻¹)	Col. Exc. Out Rate (s⁻¹)	Col. Deexc. Into Rate (s⁻¹)	Col. Deexc. Out Rate (s⁻¹)	3-Body Into Rate (s⁻¹)	Rec. Coll. Ioniz. Out Rate (s⁻¹)
1s _{1/2}	1	0.000000E+00	4.748571E+06	2.102801E+14	0.000000E+00	2.604879E+11	6.387618E+03
2s _{1/2}	2	0.000000E+00	1.644901E+16	3.970694E+16	0.000000E+00	7.897528E+12	3.555763E+12
2p _{1/2}	3	1.070514E+16	1.656094E+14	2.613926E+14	6.505157E+15	9.865269E+12	6.521507E+12
2p _{3/2}	4	1.050680E+16	1.713595E+14	2.645944E+14	6.526429E+15	9.999658E+12	6.757153E+12
3s _{1/2}	5	7.072165E+12	2.337418E+17	5.861474E+16	2.706704E+13	5.449301E+13	2.266766E+14
3p _{1/2}	6	2.535888E+16	6.560553E+16	1.517440E+16	1.096748E+17	6.189192E+13	2.792090E+14
3p _{3/2}	7	2.479356E+16	6.624065E+16	1.516210E+16	1.083556E+17	6.295611E+13	2.869904E+14
3d _{3/2}	8	1.550322E+16	2.307481E+15	4.598277E+14	7.755267E+16	7.985361E+13	4.169908E+14
3d _{5/2}	9	1.499261E+16	1.742415E+15	3.465887E+14	7.512882E+16	8.011837E+13	4.191140E+14
4s _{1/2}	10	3.176465E+14	4.326994E+17	6.201184E+16	2.211493E+15	1.701392E+14	1.235643E+15
4p _{1/2}	11	3.139126E+16	6.954712E+16	9.603310E+15	2.273531E+17	1.899359E+14	1.431790E+15
4p _{3/2}	12	3.136488E+16	5.399925E+16	7.447877E+15	2.274242E+17	1.906045E+14	1.438485E+15
4d _{3/2}	13	2.301549E+16	4.219030E+16	5.561195E+15	1.745353E+17	2.199371E+14	1.736186E+15
4d _{5/2}	14	2.152210E+16	3.219421E+16	4.219042E+15	1.641483E+17	2.241892E+14	1.779933E+15
4f _{5/2}	15	7.234643E+15	2.340244E+14	3.045206E+13	5.531172E+16	2.265954E+14	1.804750E+15
4f _{7/2}	16	6.014924E+15	2.434743E+14	3.149599E+13	4.624309E+16	2.310353E+14	1.850654E+15
5s _{1/2}	17	5.888512E+14	5.375489E+17	6.150011E+16	5.130470E+15	3.762757E+14	3.412416E+15
5p _{1/2}	18	3.051662E+16	3.928354E+15	4.434424E+14	2.703864E+17	4.008833E+14	3.685512E+15
5d _{3/2}	20	2.468370E+16	3.554040E+15	3.876228E+14	2.262126E+17	4.743750E+14	4.511148E+15
5d _{5/2}	21	2.100769E+16	3.555593E+15	3.877724E+14	1.925252E+17	4.744390E+14	4.511873E+15
5f _{7/2}	23	1.178916E+15	2.355399E+15	2.553461E+14	1.082775E+16	4.873998E+14	4.658832E+15
6s _{1/2}	26	5.705707E+13	1.213457E+16	1.207449E+15	5.727325E+14	8.402824E+14	8.760957E+15
6g _{9/2}	34	3.705989E+14	9.093385E+14	9.010312E+13	3.725418E+15	8.453403E+14	8.820771E+15

Col. Deexc./Exc.: Collisional Deexcitation/Excitation; 3-Body Rec./Coll. Ioniz.: Collisional Recombination/Ionization.

Table C.3. Temporal interval 6.65E-14 s, aluminium plasma with the conditions $T_e = 93.3$ eV, $Z_{bar} = 6.952$, $N_{ion} = 6E+22$ cm⁻³ and $E_{rad} = 1650$ eV

P_k Symbol	P_k Number	Autoloniz. nto Rate (s⁻¹)	Autoloniz. Out Rate (s⁻¹)	Autolon.→ C Out Rate (s⁻¹)	DC Into Rate (s⁻¹)	C → DC Into Rate (s⁻¹)	DC Rate (s⁻¹)	Out
1s _{1/2}	1	1.542522E+19	0.000000E+00	0.000000E+00	0.000000E+00	0.000000E+00	3.301740E+11	
2s _{1/2}	2	4.651906E+15	0.000000E+00	4.107240E+10	0.000000E+00	9.627634E+10	1.916523E+15	
2p _{1/2}	3	1.556830E+16	1.097466E+14	1.121737E+12	1.740828E+14	1.779808E+12	9.470699E+15	
2p _{3/2}	4	1.517144E+16	1.313723E+14	1.121314E+12	2.038557E+14	1.740483E+12	9.434067E+15	
3s _{1/2}	5	1.964154E+13	1.044554E+15	1.514689E+16	2.620414E+14	3.793505E+15	7.552369E+13	
3p _{1/2}	6	3.734606E+13	5.149461E+15	1.777948E+16	1.192252E+15	4.105885E+15	1.556979E+14	
3p _{3/2}	7	2.676490E+13	4.360686E+15	1.788770E+16	9.991418E+14	4.087975E+15	1.127938E+14	
3d _{3/2}	8	2.133578E+13	7.905532E+16	1.737361E+16	1.579854E+16	3.466104E+15	1.031956E+14	
3d _{5/2}	9	1.649730E+13	7.944394E+16	1.727143E+16	1.584753E+16	3.439638E+15	7.993981E+13	
4s _{1/2}	10	2.108428E+10	3.455088E+14	4.574814E+16	4.866837E+13	6.561941E+15	1.422940E+11	
4p _{1/2}	11	4.969287E+09	1.518333E+15	5.431664E+16	2.093450E+14	7.505459E+15	3.479650E+10	
4p _{3/2}	12	5.445364E+09	1.291779E+15	5.378111E+16	1.779696E+14	7.422909E+15	3.817399E+10	
4d _{3/2}	13	3.478628E+08	3.637528E+16	5.725870E+16	4.801304E+15	7.555330E+15	2.552425E+09	
4d _{5/2}	14	3.325220E+08	3.631063E+16	5.839600E+16	4.766291E+15	7.661326E+15	2.453900E+09	
4f _{5/2}	15	2.795027E+08	8.328380E+14	3.155636E+16	1.051629E+14	4.126966E+15	2.070269E+09	
4f _{7/2}	16	2.569517E+08	8.405215E+14	3.227800E+16	1.055280E+14	4.197147E+15	1.914147E+09	
5s _{1/2}	17	0.000000E+00	7.496109E+14	1.088992E+17	8.610759E+13	1.247069E+16	0.000000E+00	
5p _{1/2}	18	0.000000E+00	6.411709E+14	1.249264E+17	7.176131E+13	1.411224E+16	0.000000E+00	
5d _{3/2}	20	0.000000E+00	1.926558E+16	1.519764E+17	2.110115E+15	1.659711E+16	0.000000E+00	
5d _{5/2}	21	0.000000E+00	1.933375E+16	1.520239E+17	2.117499E+15	1.660187E+16	0.000000E+00	
5f _{7/2}	23	0.000000E+00	1.172345E+15	1.200766E+17	1.230897E+14	1.304633E+16	0.000000E+00	
6s _{1/2}	26	0.000000E+00	1.493261E+15	2.783609E+17	1.493029E+14	2.772701E+16	0.000000E+00	
6g _{9/2}	34	0.000000E+00	3.076640E+11	1.755710E+17	2.958087E+10	1.747426E+16	0.000000E+00	

Autoloniz./DC: Autoionization/Dielectronic Capture.

Autolon. → C: Autoionization and a bound electron going to the continuum; C → DC: Dielectronic Capture of a free electron of continuum.

© 2018 Benita; This is an Open Access article distributed under the terms of the Creative Commons Attribution License (<http://creativecommons.org/licenses/by/4.0>), which permits unrestricted use, distribution, and reproduction in any medium, provided the original work is properly cited.

Peer-review history:

The peer review history for this paper can be accessed here:
<http://www.sciencedomain.org/review-history/23922>